Proton Test Guideline Development – Lessons Learned

Prepared by:
Stephen Buchner, Paul Marshall, Scott Kniffin and Ken LaBel.
NASA/Goddard Space Flight Center

For:

NASA Electronic Parts and Packaging (NEPP) Program
Electronics Radiation Characterization (ERC) Project

And

Defense Threat Reduction Agency

Date: 8/22/02

Table of Contents

1.0 General Introduction

Electronic, opto-electronic and optical components on board spacecraft must operate in a radiation environment consisting of electrons and ions that span the periodic table from H to U. Exposure to those ions may cause significant damage to the components that reduce performance and compromise the mission's success. The actual fluxes encountered vary widely, depending on the spacecraft orbit, solar activity and shielding.[BART97] In some regions of space, such as in the van Allen belts surrounding the earth, the radiation environment consists of large fluxes of electrons and protons and, to a much lesser extent, heavy ions. Electrons cause damage primarily through spacecraft charging and total ionizing dose (TID). Protons, because they are highly penetrating, relatively massive and present in large numbers, degrade the performance of spacecraft components through TID and displacement damage (DD) as well as single-event effects (SEEs).

Candidate devices for future space missions should be radiation tested to assess whether they can fulfill their intended application in the anticipated radiation environment. Because testing in space is rarely practical or feasible due to the cost, time, difficulty and uncertainty involved, radiation test engineers use specialized equipment in terrestrial laboratories to generate and measure the types of damage that occur in space. To simulate the effects of proton-induced damage, engineers use proton beams at accelerator facilities. The procedures employed during proton testing depend on both the type of device being tested and the type of radiation damage being assessed. This "Lessons Learned" document is designed to serve as a guide for the radiation test engineer who needs to perform proton testing on parts being considered for use in space. It is not intended to be a "test method" but it does contain information, such as proton energy and fluence, which will, most likely, be included in any future "test method" document. Its purpose is as a guide to alert the radiation test engineer to issues that, if ignored, could lead to problems or mistakes that are sometimes merely an inconvenience and at other times result in misleading or inaccurate conclusions.

This document begins by describing those aspects of the space radiation environment relevant to protons, such as their energy spectra and how shielding modifies the spectra. Section 3 provides a list of facilities at which proton testing can be done, and includes details about the facility, such as contact person, beam properties, travel to the facility, proton energies available etc. Dosimetry is often an issue, and Section 4 describes the three widely used dosimetry methods. Section 5 contains a listing of guidelines and lessons learned that are applicable to all kinds of proton testing, such as the implications of testing in air, radiation safety issues, use of apertures, proton-induced radioactivity, etc. Sections 6, 7 and 8 are all structured similarly. Each section begins with a detailed description of the mechanisms contributing to single-event effects (Section 6), total ionizing dose (Section 7) and displacement damage dose (Section 8). Following the introduction, each section contains a list of "lessons learned" specific to that type of test. Section 9 consists of a series of "Case Studies" that illustrate some of the difficulties encountered in proton testing, such as the combination of total ionizing dose and displacement damage effects, or the effects of total ionizing dose on single event upset sensitivity. The final section contains a summary and conclusions.

2.0 Space Radiation Environment

Before proceeding, it is instructive to consider an example of the space radiation environment where the proton flux is known to exceed the heavy ion flux by many orders of magnitude. This will illustrate why proton testing is important. Knowledge of the environment is essential for predicting whether a device will survive the anticipated maximum flux and total fluence a space mission is expected to encounter. A comprehensive discussion of the radiation environment in space is beyond the scope of this monograph, and the interested reader is referred, instead, to a number of excellent reviews. [BART97, DALY01, GARR93].

Figure 2.1 presents the proton spectrum calculated for low earth orbit (705 km altitude and 98^o inclination) behind various thickness of Al shielding. The unshielded spectrum was obtained using NASA's AP8-MAX program.[BART97,SAWY76] The modified spectrum, following passage of the protons through the aluminum shielding, which represents the shielding afforded by the spacecraft itself, was calculated using another program, NOVICE. [JORD76] Notice that, in the absence of shielding, low-energy protons dominate and the spectrum extends out to a few hundred MeV. With increasing shielding thickness, the low-energy proton fluence is significantly reduced, while the fluence of protons with energies greater than 50 MeV is hardly affected. Evidently, shielding reduces the total proton flux by preferentially reducing the contributions from low-energy protons that increase the average proton energy. As a result, the choice of energies at which to test for TID, DD and SEE are partly determined by the amount of shielding. Although shielding is effective at reducing the fluence of low-energy protons, secondary radiation is generated as a result of protons interacting with the shielding material. Secondary radiation takes the form of gamma rays, neutrons, protons, electrons, alpha particles, and heavier nuclei whose distributions depend on the initial proton energy and type of shielding material. Heavy metals, such as molybdenum or tantalum, sometimes used for shielding give rise to a greater flux of secondary particles. These secondary sources of radiation may make significant contributions to DD (up to 25%) and TID (up to 7%) in shielded devices and should therefore not be ignored.[JUN01, JUN01b] Based on this discussion, it is a good idea to obtain the shielded proton spectrum prior to doing proton testing to use as a guide in the selection of proton energies.

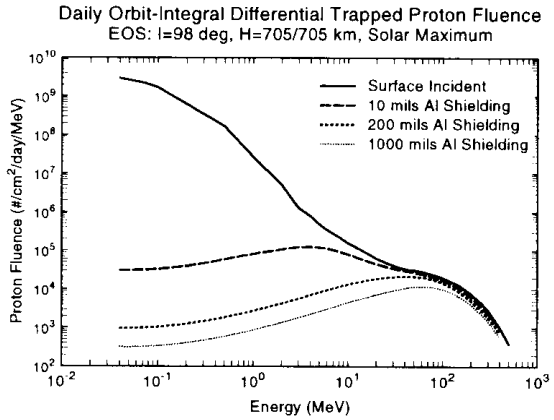

Fig. 2.1 Trapped proton fluence for low-earth orbit as a function of energy for a number of different thicknesses of aluminum shielding.[BART97]

The role of shielding in modifying the proton energy spectrum can be understood by inspecting Fig. 2.2, which shows how the proton's energy loss per unit length (dE/dx) via ionization in aluminum depends on the proton's energy. At low energy, the proton's energy loss increases rapidly until it reaches a maximum at 100 keV. Above 100 keV, the energy loss

decreases monotonically. Highly energetic protons lose relatively small amounts of energy compared with low-energy protons. For a given shielding thickness (a few millimeters), high-energy protons will lose much less energy than low-energy protons. In fact, many of the low-energy protons will not make it through the shielding, whereas the high-energy protons will pass through with a relatively small reduction in energy. As a result, the proton energy spectrum will exhibit a preferential reduction in the number of low-energy protons, the relative size of the reduction depending on the thickness of the shielding material and on the flux of secondary sources of radiation.

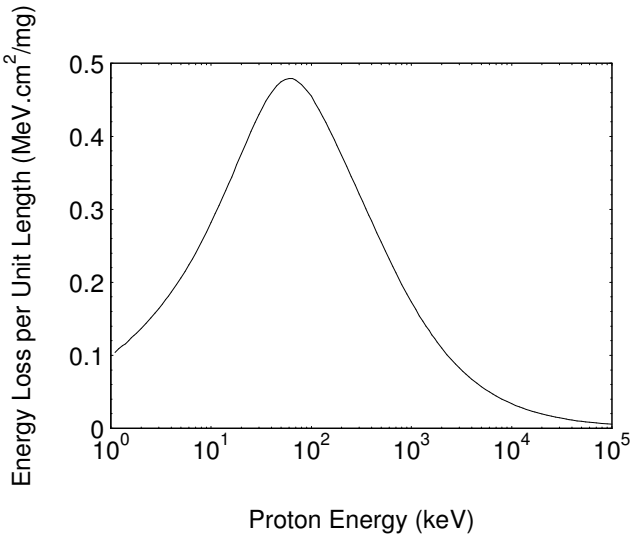

Fig. 2.2. Proton energy loss in Si as a function of proton energy

Figure 2.3 shows how shielding reduces the total ionizing dose deposited by protons and electrons in a device in low-earth orbit with altitude of 500 km and inclination of 51.6 degrees.[MARS99] Included in this calculation are the contributions from secondary sources of radiation. The figure clearly demonstrates that, for this case, increasing the shielding beyond 300 mils is not effective in reducing the dose, because the high-energy protons are not eliminated by shielding. Because shielding cannot completely protect devices against proton-induced TID, DD or single-event effects, engineers are forced to do proton testing based on the shielding modified proton spectrum at the device.

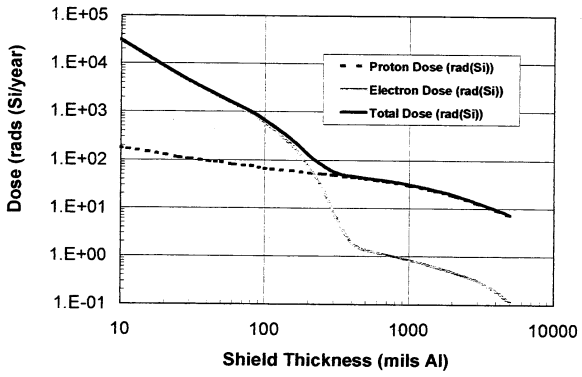

Fig. 2.3. TID due to protons and electrons as a function of shielding thickness.[MARS99]

An engineer's decision to do proton testing is typically motivated by one or more of the following factors [MARS99]:

There is no SEE or DD data available for parts that are going to be used in a proton-rich environment.

Heavy-ion data suggests that the parts might be SEE-sensitive to protons because of relatively low LET thresholds.

The parts are COTS devices, which frequently have large lot-to-lot variations in the degree of DD degradation.

The parts are in packages that cannot be de-lidded, making heavy ion testing impossible, and one would like to get a general idea of their sensitivity to SEEs.

There is neutron data on DD indicating marginal performance.

The parts may be sensitive to both TID and DD so that testing with ^{60}Co will not give the complete picture.

It is suspected that the parts may be sensitive to proton-induced SEEs via direct ionization as is frequently the case for optical detectors used in fiber optic data links or optocouplers.

There is a possibility that the parts are sensitive to proton-induced latchup, which, in many cases, is a "show stopper."

Once the decision to do proton testing has been reached, the engineer proceeds to the next stage, which is to generate a test plan. At present there is no standard test plan for proton testing, so it is up to the engineer to generate one. In the planning stage that precedes proton testing, the engineer should consider the list of issues, detailed below. That list is culled from proton testing experience gained over a period of many years. As such, the items constitute a list of "lessons learned" that should prove useful to someone, particularly the novice, wishing to do proton testing. Some may seem obvious, but ignoring them could lead to inconvenience, delay and wasted money. Before proceeding, the importance of generating a proper test plan prior to proton testing is once again stressed.

3.0 Proton Test Facilities

The facilities available for proton testing can be divided into those that provide high-energy protons with energies greater than 20 MeV and those that provide low-energy protons with energies less than 10 MeV.

3.1 High-Energy Test Facilities

3.1.1 University of California, Davis

- Crocker Nuclear Lab: http://crocker.ucdavis.edu/
- Contacts: Dr. Carlos Castaneda 530-752-4228, http://crocker.ucdavis.edu/cnl/people/staff.htm
- Accelerator: Isochronal Cyclotron
- Energies: 1-68 MeV tunable, He beam is also available, degraders available. Beam intensity adjusted by accelerator operator.
- Beam Information: single user, beam spot is 3 cm radius or collimators for smaller size and in other shapes, 22.5 MHz – 7 MHz AC, full pulse is 44.4 ns (high E) to 143 ns (low E), p+ pulse width is 1.5 ns, independent of energy
- Beam Location: Beam in air, in vault. Table for mounting experiments gives controlled motion only vertically. Alignment of target achieved with pointer and with laser beam. Not controllable remotely.
- User Interface: Computer driven by user, very user friendly
- Additional Facilities for Users: electronics shop and machine shop with techs are available to users
- Work Area/Cabling: lab area with direct access to cable run, cable run of ~60 feet
- Dosimetry: direct current read from foils compared with respect to faraday cup to calculate #particles and then dose secondary electron emission monitors
- How do you get there? Fly into Sacramento and drive WSW (about 20 minutes) on I-80 South to Davis.

3.1.2 Texas A&M University (TAMU)

- TAMU: http://cyclotron.tamu.edu/ and http://cyclotron.tamu.edu/ref/index.htm
- Contacts: Dr. Henry Clark and Dr. Vladimir Horvat: 979-845-1411
- Accelerator: K500 super conducting cyclotron
- Energies: 8 – 70 MeV tunable and degraders in line. Beam intensity adjusted by accelerator operator.
- Beam Information: single user, beam spot is 1" diameter, 20 MHz AC beam, 50ns pulse with ns p+ pulse
- Beam Location: Beam in air, in vault or in 30"D x 30"H vacuum chamber. http://cyclotron.tamu.edu/ref/layout.gif
- Also see: http://cyclotron.tamu.edu/ref/in-air.htm and http://cyclotron.tamu.edu/ref/chamber.htm
- User Interface: Fully computer driven by user (SEUSS program) or accelerator operator controlled.
- Additional Facilities for Users: electronics shop and staffed machine shop are available to users
- Work Area/Cabling: cable run of 30 feet for in air irradiation or 4 feet for vacuum chamber irradiation.
- Dosimetry: Four/Five scintillator array. See: http://cyclotron.tamu.edu/ref/measure.htm. A qualitative profile check with radiochromic film can be done upon request.

- How do you get there? http://cyclotron.tamu.edu/ref/local.htm
- Facility refs: http://cyclotron.tamu.edu/publications.html and http://cyclotron.tamu.edu/progress/2000-2001/5_2.pdf

3.1.3 TRIUMF

- http://www.triumf.ca/homepage.html & http://www.triumf.ca/welcome/
- Contacts: http://admin.triumf.ca/ Dr. Ewart Blackmore 604-222-7461
- Accelerator: Cyclotron (for more facility information see: http://www.triumf.ca/pif/)
- Energies (Tune or Degraded): 60 MeV – 500 MeV on two lines with variable energy extraction 65 to 120 MeV (line one) & 180 to 500 MeV (line two); degraders to cover gap and down to 20 MeV; two lines in the same vault, both simultaneous and completely independent with fluxes of 100 to 10^8 or 10^9 p/cm^2/s (smaller beam spot for 10^9)
- Beam Information: dual user with simultaneous variable energy extraction, 2"x2" uniform beam spot, high E line ~3"x3", 25 MHz AC, 43 ns pulse with 4 ns p+ pulse, and 10μs hole every 1ms for diagnostics
- Beam Location: closed vault, XY remote control table, rotation is manual, 4'x4' area in the room for equipment, beam at 54" high
- User Interface: both lines have computer controlled user interface and low energy line has super fine control (used for medical applications)
- Additional Facilities for Users: staffed machine shop and electronics shop, stores as well (cables and connectors)
- Work Area/Cabling: 20'x40' with some equipment and tables in this area, 65' cabling run
- Dosimetry: primary: ion chambers calibrated against externally calibrated ion chamber, secondary: faraday cup for up to 200 MeV there is a 500 MeV but infrequently used, and third: plastic scintillators, all agree very closely
- How do you get there? Fly direct to Vancouver or fly to SeaTac, WA and drive. **Don't forget your passport**.
- http://www.triumf.ca/welcome/directions.html
- Facility Note: Beam time is scheduled very far in advance. Beams run April to December, usually closed January to March for upgrades. Time on the low-energy beam line is usually more available.

3.1.4 Indiana University Cyclotron Facility

- http://www.iucf.indiana.edu/
- Contacts: Dr. Charles Foster (812) 855-2931 or (253) 565-2574, Facility: (812) 855-9365, FAX (812) 855-6645
- Accelerators: Cyclotron/Synchrotron (Cyclotron only for SEE and TID) Synchrotron gives pulses of $1x10^{10}$ p+
- Energies: 230MeV peak and can be tuned or use degraders. Beam intensity adjusted by accelerator operator.
- Beam Information: single user with beam sharing planned for future (ms time scale AM, PM continuous), up to 7cm diameter beam spot with collimators available, the beam is 35MHz with pulses on 2nd or 3rd harmonic: 50 to 100ns pulse with 0.4ns p+ pulse, future macrostructure for beam splitting will be on the order of ~100ms on, ~400ms off

- Beam Location: Beam in air, in vault. X-Y translator (remote control) with manual rotation vise, second beam line with beam sharing in future (new one will have a larger beam spot), both lines available at the same time for radiation effects work
- User Interface: Extensive user beam control computer (Beam Monster) with complete automatic control over beam and calculates dosimetry.
- Additional Facilities for Users: auxiliary electronic equipment available, limited access to machine/electronics shop
- Work Area/Cabling: 24'x10' work area, new beam line area similar size, area for setup and tear down of crates, < 100' cabling run
- Dosimetry: Faraday cup and secondary electron emission monitors, qualitative profile check with gafchromic film
- How do you get there? Go to the following web page to obtain directions http://www.iucf.indiana.edu:1080/IUCF/users/travel/VISPOLY.HTM
- Travel Coordinator: Teresa Jones, (812) 855-0485 or e-mail at teresa@iucf.indiana.edu

3.1.5 Lawrence Berkeley Laboratories (LBL)

- http://www-nsd.lbl.gov/LBL-Programs/nsd/user88/
- Contacts: Dr. Rocky Koga and Dr. Peggy McMahan (510)-486-5980 p_mcmahan@lbl.gov
- Accelerator: 88" K120 Cyclotron
- Energies (Tune or Degraded): 1-55MeV tuned
- Beam Information: single user, up to 4" diameter beam spot collimators available, 5 – 14 MHz, 200 – 71 ns pulse with a 5 – 10 ns p+ pulse
- Beam Location: vault (cave)
- User Interface: Computer driven user interface with dosimetry calculation program
- Additional Facilities for Users: staffed electronics shop (8-4) and machine shop (7-6) user accessible at other times
- Work Area/Cabling: 6' x 6' with expansion possible, cable run is variable but 30'max
- Dosimetry: ion chamber with rings for uniformity check, and radiochromic if needed
- How do you get there? Go to main web page and click USER GUIDE.

3.1.6 Harvard Cyclotron Laboratory

- http://neurosurgery.mgh.harvard.edu/HCL/

3.1.7 Loma Linda University Medical Center

- http://www.llu.edu/proton/

3.1.8 Other Facilities

- There are also several Government facilities at National Laboratories (e.g. LANL, ORNL). If your project has a military or space defense application, these facilities provide avenues you might wish to pursue. However, access to these types of facilities is very limited due to the aforementioned reasons.

3.2 Low Energy Facilities

- There are numerous low energy facilities in the United States. A comprehensive list is not within the scope of this document. We provide the NASA GSFC facility as an example of what is available.

3.2.1 NASA GSFC

- http://radhome.gsfc.nasa.gov/radhome/ref/GSFC_REF.html
- Contacts: Steve Brown 301-286-5795
- Accelerators: two Van de Graaff accelerators, one solid-state accelerator
- Energies (Tune or Degraded): both Van de Graaff accelerators are 100 keV to 1.7 MeV tuned; the solid-state accelerator is tuned from 1 keV to 130 keV for a number of elements and protons
- Beam Information: single user, all three are DC continuous beam
- Beam Location: Van de Graaff accelerators are in vaults; one beam is in air or vacuum chamber, the second is in vacuum chamber only, the solid-state accelerator is in a room with a vacuum chamber
- User Interface: accelerator operator controlled
- Additional Facilities for Users: electronics shop available, limited machining capability
- Work Area/Cabling: both Van de Graaff accelerators have about 16'x 8' of experiment space, the solid-state accelerator has 12'x8', with more available if needed for all three accelerators. Cable runs are ~65' for the damage Van de Graaff, 40' for the calibration Van de Graaff, and 3-10' for the solid-state accelerator.
- Dosimetry: calibrated solid state barrier detectors

3.3 Other Facilities Links

Below are web links to lists of other facilities in the US an abroad.

- Accelerator Labs Around the World: http://home.earthlink.net/~whittum/vl/labs.html
- LINAC96 list of LINACs and related facilities: http://linac96.web.cern.ch/Linac96/Linacs.html
- Virtual Library of Accelerator User Facilities

4.0 Other Facilities Links

High-energy facilities rely on three primary dosimetry systems to determine the flux and uniformity of the beam - scintillators (usually plastic/organic), secondary electron monitors and Faraday cups. Additionally, radiochromic films may be used to determine qualitatively beam uniformity. It is widely accepted that the dosimetry at most proton accelerators is reasonably accurate, at least within 10%.

4.1 Scintillators

A scintillator detector is a device which, when exposed to ionizing radiation, converts a portion of the incident particle energy into light. The scintillator response is directly proportional to the energy lost by the incident particle. Photons produced in the interaction are detected by a photomultiplier (PM) tube, which produces a current proportional to the light intensity. The light is absorbed by a cathode consisting of a low work-function material at the front surface of the PM tube. Electrons are emitted from the cathode and accelerated to the first anode by the electric field in the PM tube. Additional electrons are emitted by the anode and are accelerated to the next anode at higher potential. There is a series of such anodes that together give a large amplification or gain of the original signal. The gain can be greater than 10^6. The end result is a detectable electrical signal from even a single photon.[KNOL89] The scintillation detectors are placed in an annular arrangement with respect to the beam for real time monitoring of the flux. Usually four scintillators are used (top, bottom, left and right). Additionally, a fifth one may be used that is moved in and out of the center of the beam for tuning and for a more precise determination of the flux. It is not uncommon for these scintillators to be made by the facility.

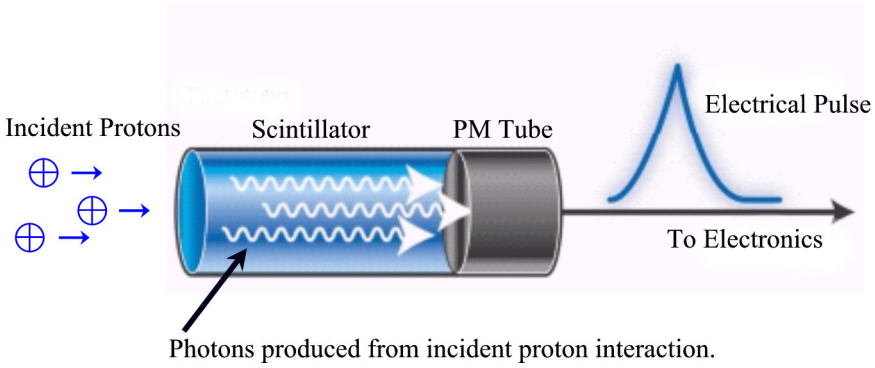

Figure 4.1. Representation of the function of a plastic scintillator. A portion of this image is from: http://www-numi.fnal.gov:8875/public/poster6.pdf

4.2 Secondary Electron Monitors

These detectors function by passing the beam through a series of thin metal films (e.g. aluminized Mylar). Interaction with the beam knocks secondary electrons free in the aluminum foils, which are tied to a picoammeter. The current is proportional to the number of ions passing through the foils. An alternate setup that allows for the determination of the profile of the beam is possible as well. The foils are arranged such that alternating foils are positively biased and the foils for detection are sandwiched in between these foils and are only aluminized on the top, bottom, left or right half. The display of the readings of each allows the operator to determine the beam uniformity and focus.[CAST01]

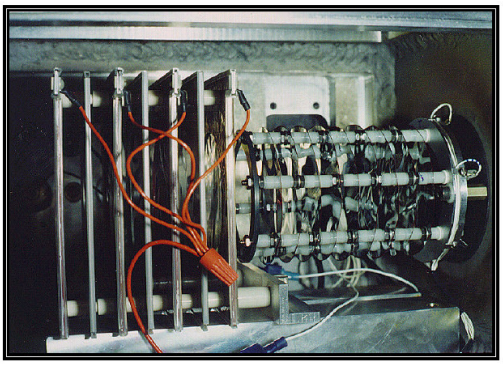

Figure 4.2: Example of secondary electron monitors used at UCD Crocker Nuclear Labs [CAST01]

4.3 Faraday Cup

The Faraday cup is as simple as it is elegant. The Faraday cup is essentially a well surrounded by a magnetic field designed to capture the entire beam. In the case of protons, for each ion entering the cup, an electron is pulled from ground through a current meter. The magnetic field around the cup prevents secondary electrons inside the cup from escaping and prevents any produced externally from entering. Faraday cups are designed to be moved in and out of the beam or are placed in a separate area to provide measurements only when needed. An example of a motor driven one is provided below.

Figure 4.3. Picture and schematic of Faraday cup.
Image from: http://www.casetechnology.com/implanter/faraday.html

4.4 Radiochromic Films

Radiochromic films are frequently available for on-demand testing of a beam's uniformity in a purely qualitative manner. The film is exposed to a dose known not to saturate the film. The film is then read by any number of means, but the most popular method is to scan the film with a simple flatbed scanner into a grayscale (0-255) image, and process it with a commercially available software package. One such program is Scion Software, available at

www.scioncorp.com. While this software package was originally developed for use in scanning PCR films in DNA research, it is well suited for use in this application. The software includes the ability to look at a 3D plot of the beam spot and to do a histogram of any cross section of the film desired. Non-uniformities in the beam are immediately obvious.[CAST01],[JONE99]

4.5 Beam Degraders

It should be noted that if a degrader is positioned in front of the DUT, the dosimetry is altered. The user must make the necessary corrections to allow for the broadening and shifting of the peak in the energy spectrum as a result of energy loss that depends on the type of material used in the degrader as well as its thickness. For more on the use of degraders, see Sections 5.15.1, 5.16, 6.2.1, and 6.5.3.

5.0 General Lessons Learned

Lessons learned that are of a general nature and apply to all types of proton testing, including SEE, TID or DDD are detailed in this section. They include radiation safety, device alignment, remote control of the experiment, range calculations, shipping equipment and booking time.

5.1 Radiation Safety

Radiation safety is of paramount importance because of the serious health hazards resulting from exposure to the radiation present during proton testing. Testing is accomplished by placing the DUT in front of an exit port on the test chamber. The protons reach the DUT after passing through a thin membrane from the vacuum into air and both the primary protons and the secondary particles, such as neutrons, generated when the protons collide with any material, pose a significant health hazard. Another source of radiation is the material activated by the protons with a half-life that depends on the type of material – materials composed of low Z elements, such as Al, generally have short half-lives (minutes), whereas heavy materials, such as Au, will have much longer half-lives (days). The dangers associated with exposure to radiation preclude anyone from being present in the vault when the beam is on. Once the beam has been turned off, the radiation test engineer should enter the room with a Geiger counter to monitor the radiation level. (Note that the danger to humans is related to the radiation dose, which is the product of proton flux and exposure time.) Because of the legal issues involved, no safe exposure levels are given in this monograph, and the test engineer is advised to consult the radiation health physicist at the facility if any issues arise. Before being allowed into the vault, some facilities require that the test engineer take a rudimentary radiation safety course that consists, at a minimum of a description of what to do in an emergency. (Although not required in the United States, some European proton test facilities require test personnel to have a radiation physical prior to doing the test. Without the relevant documents proving that you have had a radiation physical, you will not be allowed to perform radiation testing.) All facilities require anyone entering a radiation facility to wear a radiation "badge" at all times to monitor total radiation exposure. Make sure the facility gives you one before you begin to work in any areas marked as a potential radiation hazard.

5.2 Safety Interlocks

After the experiment has been set up and everything is ready, the last thing to do is to set the safety interlocks. They are designed to ensure that no one is inadvertently left in the vault after the door is closed. In some facilities there are flashing lights and in others loud beeping sounds signaling that the interlocks have been activated. Make sure an accelerator staff member shows you how to operate the interlocks and explains what to do if you are inadvertently left in the testing room. Failure to activate the interlocks prior to leaving the vault will prevent the beam stop from being removed and no testing can be done until the interlocks have been set correctly. All facilities have a "panic" button in the vault so that if, by chance, the beam is turned on while someone is still in the vault, touching the button will immediately switch the beam off.

5.3 Positioning the Device Under Test (DUT)

The board containing the DUT must be securely mounted in front of the exit port. One method is to clamp the board in a vice provided either by the facility or the radiation test engineer. Avoid clamping where there are exposed electrical wires or connectors that could short out through the metal vice. At UCD, the vice sits on a table that can move in the vertical direction. Movements in the x and y directions are done by hand. The vice must, in turn, be secured to the table using, for example, C-clamps. Proton testing at non-normal incidence is only rarely done so that few facilities have stages capable of rotating the DUT while still keeping it in the center of the beam. If testing at non-normal incidence is necessary, you might have to bring along your own goniometer. Alignment is critical to make sure the DUT is positioned in the

center of the beam, where uniformity is best, particularly when the DUT is rotated away from normal incidence. At UCD alignment is achieved either with a mechanical pointer attached to the cover that protects the port window or with vertical and horizontal laser beams that cross at the center of the beam.

5.2 Use of Apertures

Apertures are used to limit proton-induced damage to other devices adjacent to the DUT. They fit over the exit port and consist of thick aluminum covers that contain holes of various sizes and shapes to limit the extent of the beam. It is advisable to use the apertures even when there are no other devices adjacent to the DUT. The apertures limit exposure to the proton beam of both the board to which the device is attached and the mounting hardware, and so minimizes activation of heavy metals, such as gold, used on the board. After high proton fluences, the apertures are activated and should not be handled until the radioactivity has decreased to acceptable levels.

5.3 Remote Control of the Experiment

As already mentioned, the presence of high fluxes of radiation in the radiation exposure room requires that engineers not be present during testing. Therefore, DUTs must be controlled remotely using long cables passed through tubes in the thick concrete walls of the vault. For experiments at UC Davis and IUC, the cables need to be about 50 feet in length. In addition, most facilities have patch panels with BNC connectors both inside and outside the vault. The BNC connectors are labeled to facilitate connecting test equipment inside the vault with other equipment, such as computers, in the room where the test engineers sit. Various approaches can be used for remotely controlling the DUT, such as local area networks or bus extenders. Some facilities have CCD cameras in the radiation exposure room that are connected to monitors located where test personnel work during a test run. They can be used, for example to monitor the current supply for a DUT because increases in supply current are one manifestation of TID degradation. (See Section 7.1) This is often easier than monitoring a power supply outside the radiation exposure room, for which the voltage drop along a long cable (~50′) must be considered.

5.4 Exposure in Air

The rate of energy loss in material for high-energy (>20 MeV) protons is sufficiently low that testing can be done in air. The proton beam travels down the vacuum tube to the exit port where it passes through a thin window and intervening air gap with minimal energy loss. The fact that the exposure takes place in air greatly facilitates testing devices that require cooling because a fan is often sufficient to cool the DUT, thereby avoiding the use of water cooling in a vacuum. In addition, DUTs can be exchanged relatively quickly because it is not necessary to bring a vacuum chamber up to air and then pump it down again. The energy lost by the protons passing through the window material and the air between the window and the DUT must be taken into account at low proton energies (below 20 MeV). The presence of the thin window membrane on the accelerator exit port mandates that great care be exercised when aligning the DUT so as not to puncture the membrane. If the membrane is punctured, there will be a loud implosion as the vacuum is rapidly lost. This could result in damage to both the accelerator and the DUT as well as injury to the test engineer. Furthermore, there would likely be a significant delay before the accelerator could be brought on-line again, a delay that could prevent any more testing during the scheduled time. To avoid breaking the thin film, the exit port should be kept covered during alignment and the cover removed only at the very last moment. Forgetting to remove the cover is a frequent mistake, and although it does not do anything to the device, it can waste precious time. This frequent error can be avoided by aiming a CCD camera in the vault to include the exit port to facilitate checking remotely whether the cover has been removed. This avoids having to go

back into the chamber after all the safety interlocks have been set and the door closed to check whether the cover is still on the exit port.

5.5 Protection of Support Equipment

Scattered radiation, including neutrons and protons, present in the chamber during testing can damage sensitive equipment used to exercise the DUT, especially if the equipment is located close to the proton beam. Any equipment required to be in the radiation chamber should be positioned away from the beam, and shielded with good neutron absorbers, such as lead bricks or boxes of Borax. This precaution is particularly important when high proton fluences are anticipated or when the equipment is to be used for many experiments. Figure 5.1 shows how boxes of Borax have been placed to protect an expensive power supply. Borax contains boron, which has a high absorption cross-section for neutrons, making it an effective neutron absorber.

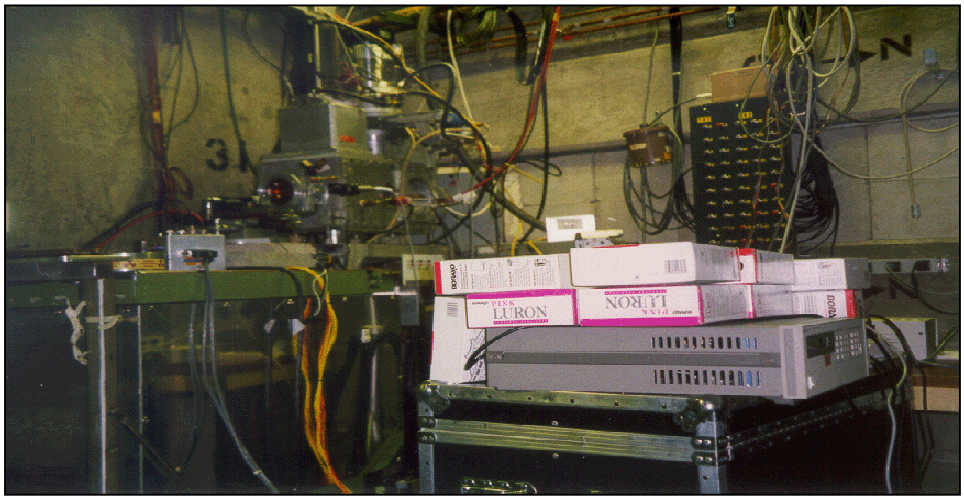

Fig. 5.1. Boxes of Borax being used to shield the power supply against stray neutrons during proton testing at UC Davis.

5.6 Secondary Neutrons

The proton beam striking the DUT is contaminated with neutrons generated as a result of protons interacting with the foils of the secondary electron emission monitor (SEEM), the window material and air molecules between the window and the DUT. The neutron flux is typically four orders of magnitude lower than the proton flux so that its contributions to radiation damage of the DUT are usually ignored. [BERG97] Only where there is thick shielding consisting of heavy metals do neutrons make a significant contribution.

5.7 Beam Control

In some cases, such as at UC Davis, the control room hands over limited control of the beam to the test engineers. The test engineer determines when to turn the beam on and off, and also calibrates the SEEM and corrects for electronic noise in the SEEM. The control room maintains control over the flux, which is specified prior to the run by the test engineers. The control room also removes and inserts the beam stop at the beginning and end of each run. When the beam stop is out, entry to the experimental chamber is forbidden. Request that a staff member show you how to use the computer. You should also ask the staff member to explain how to continue a run following a sudden drop out of the beam, which happens on occasion. Following a run, the beam parameters, including dose, fluence, exposure time, average beam current, etc should be recorded either as a hard copy or on floppy disk. Bring along a storage medium such as a floppy

disk to store the file. At other facilities, such as IUCF, accelerator personnel control all aspects of the irradiation and provide a hard copy of beam statistics for each run. TAMU will e-mail the files.

5.8 Proton Energy Specification

The proton energy available from a cyclotron depends on the cyclotron frequency, which is set by the accelerator operator. Before it reaches the DUT, the protons first pass through a metal foil to scatter the beam so that it covers a larger area and has improved uniformity. There is a small energy loss as it passes through the foil. Next, the beam passes through a secondary electron emission monitor (SEEM) consisting of a series of metal foils used to measure the beam flux, and again there is a small energy loss. The beam then passes through the window material and finally through a few centimeters of air before reaching the DUT. As an example of the energy loss, the proton energy at UCD drops from 67 MeV in the accelerator down to 63 MeV at the DUT if the DUT is positioned at the location indicated by the pointer on the exit port cover. Make sure that when you specify the proton energy you know which one you are specifying.

5.9 Induced Radioactivity

The use of heavy metals in test fixtures should be avoided because they have long radioactive half-lives when activated. Aluminum is the material of choice because of its short half-life. Parts containing heavy metal that have been tested to high fluences may require considerable time before they can be safely handled. In particular, radiated devices that are radioactive cannot be removed from the site and must remain there until they can be shipped. Consult accelerator facility personnel. At the end of the experiment, most facilities require that all devices exposed to the proton beam be tested for radioactivity, so do not pack any DUTs until their radioactivity has been tested by facility personnel.

5.10 Food and Drink

Because of the potential of radiation contamination, food is not allowed in any areas where there is a possibility of radioactive dust settling on the food. Keep food outside the experimental chamber. Furthermore, if you have worked in the experimental chamber, it is a good idea to wash your hands to remove any activated dust before handling any food.

5.11 Shipping

Bring along prepaid shipping documents so that your equipment can be returned on time. Most facilities are helpful when it comes to return shipping. However, if you anticipate finishing up late at night when there is no staff in the office, arrange for return shipping during the day, before the staff go home.

5.12 Booking Time

It is important that you contact the accelerator facility well ahead of the anticipated testing date, because beam time is frequently at a premium. Furthermore, you may not be able to do any testing without a contract in place with the facility. Contract sometimes takes months to finalize and it is important that the process be started well ahead of the test data.

5.13 Beam Parameters

For any experiment it is necessary to specify proton energy, flux, uniformity and fluence.

5.13.1 Energy

The proton energy used for testing is determined by the type of experiment (SEE, TID or DD) and will be discussed in greater detail in the appropriate section. The proton energy can be set either by tuning the cyclotron's frequency or by placing degraders in the beam.

Degraders are slabs of material that reduce the proton energy by a fixed amount depending on the slab's thickness and composition. Degraders are best made from low Z material such as Al and Lexan to minimize activation. As will be pointed out in section 5.16, straggle must be considered, especially if thick degraders are used to reduce the proton's energy by a large fraction.

5.13.2 Flux

Flux is determined in part by the cost of beam time and by the capacity of the test equipment to gather the relevant data. This will be discussed in greater detail in later sections. The flux is determined by the beam current, which is measured in amperes. The average proton current at UCD ranges from about 0.1 pA ($2x10^4$ particles/sec/cm^2 or 2 mrads(Si)/sec for 63 MeV protons) to 100 nA ($2x10^{10}$ particles/sec/cm^2, equivalent to a dose rate of about $2x10^3$ rads(Si)/s). The minimum flux is limited by the SEEM. The SEEM measures current that flows between two sets of foils in the vacuum. Protons passing through the SEEM eject electrons that are collected by foils maintained at positive bias. If the noise in the SEEM is comparable to the beam current, the accuracy of the dosimetry is compromised. On the other hand, very high proton fluxes (>10^{10} /cm^2) are known to heat the DUT, which may affect parameters being monitored. For instance, heating can affect the annealing rate of TID damage.

5.13.3 Uniformity

Beam uniformity is important, particularly if more than one device at a time is to be tested, or if the device is comparable in size to the beam. The accelerator operator should measure beam uniformity at the beginning of a run using radiochromic dye film. After exposure to a predetermined proton fluence, the radiochromic dye film is scanned to determine uniformity. From the scanned figure, corrections to the fluence as a function of distance from the center

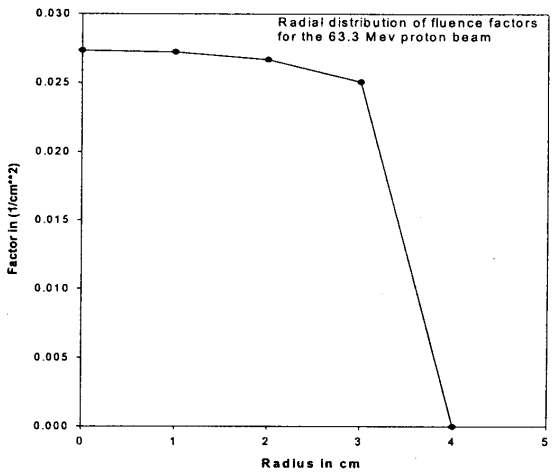

Fig. 5.2 Correction factors used for the UC Davis proton beam as determined by scanning of a radiochromic dye film.[CAST01]

of the beam can be obtained. Fig. 5.2 shows the correction factors used at UC Davis.[CAST01] The figure shows that within a radius of 2 cm from the center of the beam, the fluence varies by about 5% and within a radius of 3 cm it varies by about 10%. Beam uniformity is also monitored in "real time" by the accelerator operators using an array of four scintillator detectors placed around the edge of the beam. If the beam drifts, small adjustments can be made to return it to its optimum position.

5.13.4 Fluence

Prior to starting an exposure, the test engineer should have an idea of the fluence required for a particular test based on the predicted fluence the part is expected to experience in space. Because of margin requirements, the parts are usually tested to fluences greater than what they will be exposed to in space. There are two approaches to testing. In the first, the fluence or dose is applied in incremental steps and the part tested after each step. This is usually necessary when doing single-event upset (SEU) testing, or TID testing when checking the DUT for damage takes such a long time to complete that after checking the device will have accumulated a significant increment in dose. The TID damage is then plotted as a function of either fluence or dose. The second method involves monitoring the relevant parameters during exposure. This is typically done when testing for single-event latchup (SEL). It may also be done for TID testing by continuously monitoring the leakage current. In the case of SEU testing, the total fluence is determined by statistics. For example, if one is satisfied with data having statistical error bars of 10%, the fluence should be such that at least 100 SEUs are detected, because the statistical variations typically scale as $N^{0.5}$. During SEL testing, it is frequently necessary to turn the beam off while power to the part is being recycled. Failure to do so means additional fluence would be accumulated during a period when the DUT was not sensitive to SEL. One way to avoid this problem is to keep the flux sufficiently low that very little additional fluence is added between the time the part latches and the time the beam is turned off. The facility at UCD provides hard copies of all the relevant parameters for each run, including exposure time, beam current, proton energy, run number, uniformity, incremental fluence, incremental dose, total fluence and total dose. The maximum fluence is determined by the type of test being conducted. For SEE testing, the maximum fluence is set by the desired SEE statistics, whereas for TID and DD testing, the fluence is determined directly by the environment.

5.14 Range Calculations

How far a proton penetrates through matter depends on the proton's energy and on the electronic and nuclear characteristics of the target material. The calculations are sufficiently complex that computer programs based on a Monte Carlo approach are used. One such program is SRIM2000, available free on the web. [ZIEG96] The program consists of two modules, 1) stopping power/range and 2) TRIM, which is a Monte Carlo simulation of the proton-matter interaction. The first module calculates stopping powers via ionizing and non-ionizing interactions as well as ranges of ions in matter. Table 5.1 lists the ion energy, ionizing energy loss, non-ionizing energy loss, range, longitudinal straggle and lateral straggle. The table shows that 60 MeV protons have an electronic linear energy transfer (LET) in Si of 0.008596 MeV-cm^2/mg and a range of 1.685 cm. With increasing energy, the range increases but the initial LET decreases. Fig 2.2 shows graphically the energy loss due to ionization over a much wider range than that covered by Table 5.1. The web site for Brookhaven National Laboratory's SEU facility contains a downloadable program for calculating LET for any incident ion into most target materials (***http://tvdg10.phy.bnl.gov/index.html).***

The table also shows that energy losses via nuclear interactions (that lead to DD effects) are three orders of magnitude lower than energy losses via ionization for the same proton energies. This column includes only Coulomb scattering and ignores inelastic scattering, leading to an underestimation of the total amount of DD at higher proton energies. The reader is cautioned against using it for calculations of displacement damage dose for proton energies above 8 MeV.[MARS99]

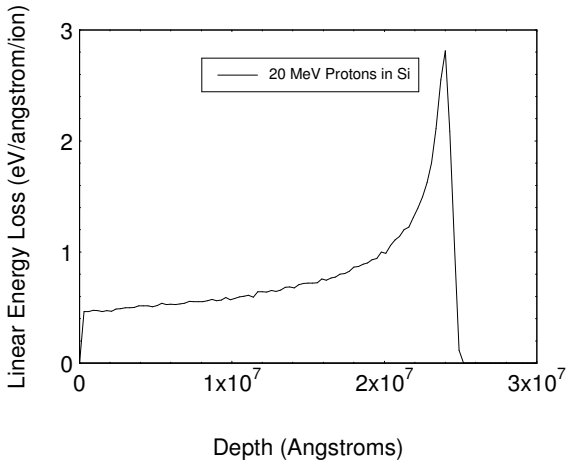

Fig. 5.3. Linear energy loss for protons in Si as a function of distance from the Si surface.

Table 5.1 SRIM2000 Output for Protons in Silicon.

Ion Energy	dE/dx Electronic	dE/dx Nuclear	Projected Range	Long. Straggling	Lateral Straggling
1.00 MeV	1.781E-1	1.328E-4	15.68 um	7591 A	9379 A
5.00 MeV	5.866E-2	3.297E-5	215.28 um	9.53 um	10.22 um
10.00 MeV	3.479E-2	1.786E-5	708.58 mm	32.69 um	31.64 um
20.00 MeV	2.029E-2	9.614E-6	2.39 mm	98.56 um	101.57 um
30.00 MeV	1.476E-2	6.677E-6	4.91 mm	212.97 um	203.18 um
40.00 MeV	1.177E-2	5.150E-6	8.19 mm	328.13 um	333.14 um
50.00 MeV	9.895E-3	4.208E-6	12.18 mm	530.91 um	489.13 um
60.00 MeV	8.596E-3	3.566E-6	16.85 mm	723.37 um	669.25 um
70.00 MeV	7.641E-3	3.100E-6	22.15 mm	916.42 um	871.86 um
80.00 MeV	6.909E-3	2.476E-6	28.07 mm	1.26 mm	1.10 mm
90.00 MeV	6.329E-3	2.467E-6	34.56 mm	1.58 mm	1.34 mm
100.00 MeV	5.857E-3	2.241E-6	41.62 mm	1.89 mm	1.60 mm
120.00 MeV	5.135E-3	1.897E-6	57.32 mm	2.50 mm	2.18 mm
140.00 MeV	4.609E-3	1.648E-6	75.01 mm	3.12 mm	2.82 mm
160.00 MeV	4.208E-3	1.458E-6	94.54 mm	3.74 mm	3.52 mm
180.00 MeV	3.893E-3	1.309E-6	115.79 mm	4.37 mm	4.26 mm
200.00 MeV	3.637E-3	1.189E-6	138.63 mm	5.50 mm	5.06 mm

The second module, TRIM, can be used to calculate the energy loss as a function of distance into the silicon. To do that one must specify that TRIM save the ionization data to a file, which can then be plotted. Figure 5.3 shows an example of the ionizing energy loss per unit length versus depth in silicon for 20 MeV protons. This information is sufficient to calculate the charge density per unit length in the charge track generated by the proton. A useful conversion factor is that a LET of 96 MeV-cm^2/mg is equivalent to a linear charge density of 1 pC/μm. This conversion factor may be used to show that a 60 MeV proton has a LET of 0.0085 MeV-cm^2/mg and produces a linear charge density of approximately 0.1 fC/μm.

SRIM2000 can also be used to calculate the average proton energy loss after passing though a finite thickness of material, information that is needed for determining the thickness of degraders used to reduce proton energy without having to retune beam energy. This can be done using the TRIM module. For instance, if one wishes to reduce the energy of a 100 MeV proton beam to 50 MeV using an aluminum degrader, a calculation of stopping power and range for 100 MeV protons in aluminum should first be done. The calculation shows that the range is 36.92 mm. Next one takes a guess for the aluminum thickness, say 20 mm, and the TRIM calculation is carried out for an arbitrary number of ions, (200 ions is a reasonable number). For the calculation, one must specify that a file containing the transmitted ions be generated. The results of the calculation show that the average energy of the protons is too high. A thicker degrader is then tried and the calculation repeated. One eventually finds that 26 mm of aluminum reduces the average proton energy from 100 MeV to 50.2 MeV. The results can also be used to calculate the energy straggle. The file generated for this calculation lists the energies of the 200 transmitted protons. The energies differ slightly because of the statistical nature of the proton-atom interactions. First the average energy of all 200 protons is calculated and then the standard deviation. In this case the straggle is approximately 2 MeV. If necessary, the stopping power and range of the 50.2 MeV protons in silicon can be calculated. Also, nuclear interactions need not be considered because the associated energy loss is about three orders of magnitude less than for ionizing energy loss.

There is another way to calculate the energy of a particle after passing through a finite thickness of material. For this approach it is best to use the program from Brookhaven National Laboratory because smaller energy steps can be selected compared with the fixed larger energy steps provided by SRIM. The smaller step sizes improve the accuracy. Table 5.1 shows how to calculate the energy of a 60 MeV proton after passing through 8.66 mm of silicon. The range of a 60 MeV proton is 16.85 mm. If 8.66 mm are subtracted, 8.19 mm are left. The table shows that the energy of a proton with a range of 8.19 mm is 40 MeV. That is the energy of the emerging proton.

5.0 Proton SEE Testing

The underlying mechanisms responsible for most proton-induced SEEs differ from those for heavy-ion induced SEEs. Heavy ions cause SEEs by direct ionization, whereas most protons first undergo a nuclear interaction and the products of the interaction subsequently produce SEEs via direct ionization. (The exceptions would be large devices, such as photodetectors, in which protons can generate sufficient charge by direct ionization to produce SEEs when they travel through the device at grazing angle of incidence). Because nuclear interactions are involved, testing for proton-induced SEEs involves measuring the cross-section as a function of proton energy, and not as a function of linear energy transfer (LET) as is normally done for heavy-ions. Only in the case of photodetectors or, possibly, advanced devices on very thin epitaxial layers are angular measurements necessary to ascertain whether SEEs occur via direct ionization. In this section we will first describe how SEEs are generated by protons and then present a list of suggestions to guide the experimenter doing proton SEE testing.

6.1 Background

When ions, including protons, pass through materials such as semiconductors and insulators, they collide with the electrons and nuclei of the constituent atoms, losing energy in the process. Protons scatter elastically off the electrons through electromagnetic forces, whereas they scatter both elastically (via electromagnetic and nuclear forces) and inelastically (via nuclear forces) off the nuclei. The largest cross-section, by far, is that for proton-electron scattering, in which the energy lost by protons liberates electrons bound to their host atom, producing free electron-hole (e-h) pairs that form a track of charge in the ion's wake. The linear charge density along the track can be calculated from the ratio of energy loss per unit length and the average energy (E_g) required to generate one e-h pair (E_g = 3.6 eV in Si). The energy loss per unit length is obtained from the normalized energy loss, termed linear energy transfer (LET), which can be obtained from SRIM2000, as discussed in Section 5.14. As a result of diffusive forces, the e-h pairs in the track spread out laterally in a matter of picoseconds before ultimately recombining or being collected at junctions.

Electric fields present in semiconductor p/n junctions and gate oxides of MOSFETs separate the e-h pairs generated by the ions, preventing their immediate recombination. The charge separation results in an electric current that disturbs the voltage at the node. If the voltage disturbance is sufficiently large, a SEE can occur. The total charge collected equals the integrated current over time or, alternatively, the product of the charge density and the collection depth. For the case of a semiconductor p/n junction, charge collection occurs from a region that includes the junction's depletion layer and an additional distance that takes charge collection (funneling and diffusion) from outside the depletion layer into account. The charge generated in the depletion layer is collected via drift in the depletion layer's electric field, causing a rapid change in the voltage across the node. Charge generated beyond the depletion layer is collected via diffusion, which is a much slower process and is driven by carrier concentration gradients. Two additional features of charge collection should be noted: first, less charge may be collected when a SEU occurs than when one does not occur [DODD95]; second, more charge may be collected than deposited making certain devices, such as GaAs MESFETs and Si transistors made on thin epitaxial layers, very sensitive to SEUs [MCMO92]. For the case of a gate oxide, the charge collected is just the product of the LET (in the oxide) and the oxide thickness. A metric used to express the sensitivity of a device to SEEs is critical charge, which is the minimum amount of charge required to produce a SEE. Devices sensitive to SEE have small critical charges, typically on the order of fC.

It follows from the above discussion that an ion's LET (the amount of charge it deposits per unit length in the material) is a good measure for judging a circuit's sensitivity to SEEs. A circuit

that exhibits SEEs when exposed to low LET ions is more sensitive than one that requires high LET ions. Consequently, the accepted way to test for a device's SEE sensitivity is to measure the number of SEEs per unit fluence (cross-section) as a function of ion LET.

Charge generated in the gate oxide of a MOSFET can cause single-event gate rupture (SEGR). Similarly, charge generated in the semiconductor, at or near a p/n junction, can cause single-event effects [SEXT92] [MASS93] such as single-event upset (SEU), single-event latchup (SEL) [JOHN96], single-event transient (SET) [KOGA93], single-event snapback (SESB) [KOGA89] and single-event burnout (SEB) [TITU96]. All these effects can, in principle, occur during proton testing.

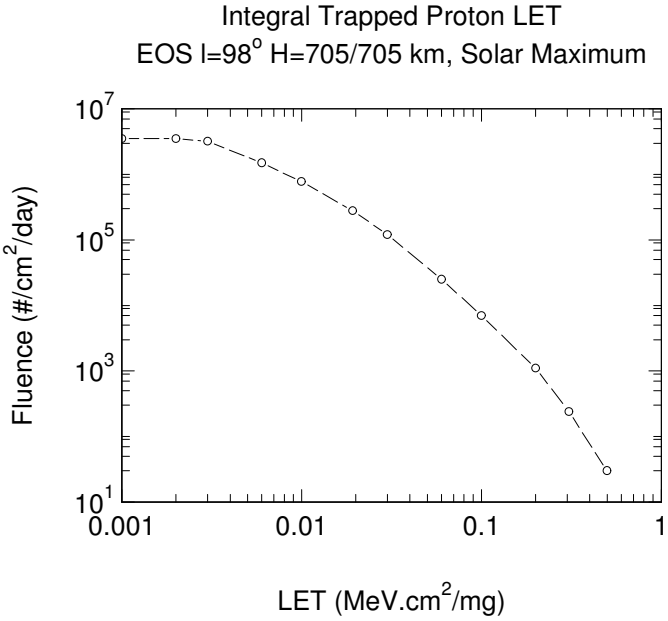

Fig. 6.1. Proton Energy Spectrum in Low Earth Orbit.

An ion's LET depends on its mass and energy as well as the material through which it passes. Protons have small LETs because of their small mass. As pointed out in Section 5.13, 60-MeV protons have a LET in Si of 0.008 MeV.cm^2/mg, and even with a collection depth of 10 μm, the total amount of charge collected is generally not sufficient to cause SEEs. Figure 6.1 shows the LET spectrum for protons in low earth orbit. Clearly, the majority of protons have LETs less than 0.4 MeV-cm^2/mg. Therefore, except for certain devices, such as photodetectors that are designed to respond to small amounts of charge and for which large collection path lengths are possible, SEEs produced by direct proton ionization rarely occur in space.

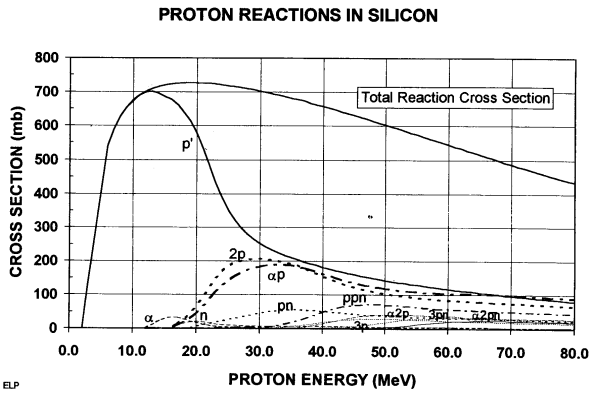

Fig. 6.2. Cross-section as a function of proton energy for elastic and inelastic scattering.[PETE96]

As already pointed out, protons can interact both elastically and inelastically with nuclei. Figure 6.2 shows the results of a calculation of elastic and inelastic scattering cross-sections. The figure shows that the cross-section is dominated by elastic scattering (p′), particularly at low energies. In an elastic interaction, protons collide with nuclei and are scattered in all directions. The nuclei move off in other directions determined by the laws of conservation of momentum and energy. Recoiling protons have very low LETs and are unlikely to produce SEEs. In contrast, recoiling nuclei, with masses much larger than protons, also have much larger LETs. The amount of energy deposited in a sensitive volume by a recoiling nucleus depends on a number of factors, including the energy of the recoiling nucleus and the thickness of the sensitive volume. As an illustration, consider the maximum energy imparted to a recoiling Si nucleus. In a collision in which the proton undergoes a change in direction of 180^o - a relatively rare event - the maximum energy imparted to the recoiling Si nucleus is 0.133 E_p, where E_p is the incident proton energy. The value $0.133E_p$ is obtained from the laws of conservation of energy and momentum in an elastic 180^o collision.[PETE97] For 60-MeV protons undergoing elastic scattering with Si nuclei, the maximum energy available to the Si nuclei is 0.133x60 MeV (= 7.8 MeV), which gives the recoiling Si nucleus has an initial LET of 12.5 MeV-cm^2/mg and a range in Si of 4.5 μm. If all the lost energy were converted to charge, the total number of electron-hole pairs generated would be $7.8x10^6/3.6 = 2x10^6$ (where 3.6 eV is the average amount of energy needed to produce 1 e-h pair in Si.) If all the e-h pairs are generated in the sensitive volume, the total collected charge is $3.2x10^{-13}$ C, or 0.32 pC, which is sufficient to generate SEEs in sensitive devices.

Another way to look at elastic nuclear scattering is to calculate the maximum LET of the recoiling Si nucleus. SRIM2000 calculations show that the maximum LET of a recoiling Si nucleus in a Si lattice is 15.23 MeV.cm^2/mg, which corresponds to a range of 9 μm. The energy of the Si nucleus with this LET is 25 MeV. The proton energy required to produce this via backscattering is approximately 200 MeV, a rare but possible event in space.

Inelastic scattering of protons may also cause SEEs. During inelastic scattering the incident protons are absorbed by atomic nuclei. The excited nuclei subsequently relax by emitting daughter particles with masses from He to Si. Although their interaction cross-sections are smaller than for elastic scattering interactions (see Fig. 5.6), they are able to deposit more energy and, therefore, more likely to produce SEEs. As an example, the maximum amount of energy available from 40 MeV protons in elastic scattering is 5.3 MeV ($1.5x10^6$ electrons) compared with 22 MeV ($6x10^6$ electrons) for a spallation reaction ($^{16}O + {}^{12}C$).[PETE96]

Figure 6.3 shows the results of a calculation for the recoil energy spectra (energy density per MeV) as a function of energy for both P -> 2P and P -> P+He+Na interactions. Which one causes a SEE depends on how the energy is apportioned between the He and Na ions. In general, as the proton energy increases, the SEE cross-section rises because the heavier ions will have more energy to deposit in the sensitive volume.

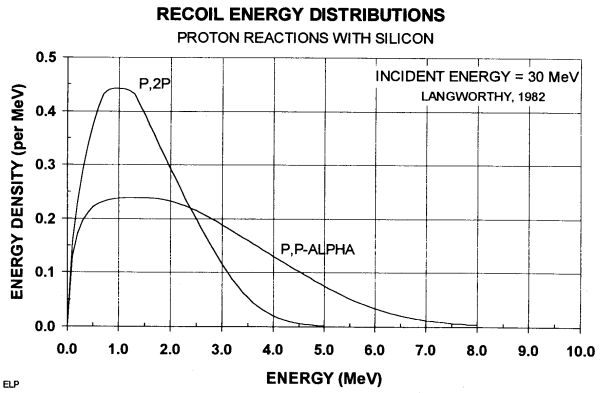

Fig. 6.3. Energy density as a function of recoil energy for inelastic scattering. One is for production of 2 protons and the other for the production of a proton and an alpha particle.[PETE97]

Although the cross-sections for these indirect ionization interactions are approximately five orders of magnitude lower than for direct ionization interactions, they dominate the error rate in proton-rich environments, such as in the proton belts, where the large proton flux compensates for the relatively low nuclear interaction cross-section. [DODD99]

The different mechanisms responsible for SEEs produced by direct and indirect ionization have experimental ramifications. In the case of direct ionization, a SEE occurs when a quantity of charge, greater than the critical charge, is deposited in a "sensitive" volume. The total charge deposited in the sensitive volume is given by the product of the LET and the path length, which varies according to the direction of the incident ion and is given by LET/cos(θ) where θ is the angle of incidence. By varying the angle of incidence, the effective LET can be varied. To calculate the error rate, one integrates the product of the differential ion LET spectrum of the environment and the integral path length distribution functions over LET. Therefore, to assess a device's sensitivity to heavy-ion induced SEEs, the SEE cross-section is measured as a function of ion LET.[DODD99]

This approach is not normally used for proton testing because in most devices SEEs are generated by indirect ionization. The incident proton undergoes a nuclear interaction with the constituent atoms, and the cross-section depends on the total number of atoms in the sensitive volume, as long as the beam is larger than the sensitive volume. Since the nuclear interaction is energy dependent, the cross section is measured as a function of proton energy. That information is then used in error rate calculations to be discussed in greater detail in Section 6.9. Furthermore, because the charge generated by direct ionization can be neglected, chord length distributions need not be considered and the measurements can be done at any angle. There is one exception where proton-induced SEEs could exhibit angular dependence. That is the case for sensitive volumes (the depletion layer of a p-n junction) which are shallow vertically and wide laterally.[REED95] Because conservation of momentum dictates that there is a preference for forward scattering, more daughter products will leave the sensitive volume when the protons are normally incident than when they are incident at a finite angle. This can lead to lower SEE rates for normal incidence than for incidence at a finite angle.

The preceding description of proton-induced SEEs provides a basis for the following sections. The tester should consider the following ″lessons learned″ as they apply specifically to proton SEE testing.

6.2 Proton Beam Parameters.

A careful selection of proton beam parameters is required to obtain valid data for predicting SEE rates in space. These include proton energy, flux, and fluence.

6.2.1 Proton Energy.

The selection of proton energy depends on what one wants to know about proton-induced SEEs. If the goal is to screen parts for single-event latchup, the highest available energy should be chosen and measurements need only be done at that energy. If the goal is to be able to predict SEU rates in space, it is necessary to measure the SEU cross-section as a function of proton energy, from threshold to saturation. (The exception would be devices containing photodetectors where SEEs may be caused by direct ionization, and for which other methods would have to be used.) The number of different energies needed depends on the following:

- Available accelerator time and the time to change proton energy (approximately an hour).
- Budget to pay for accelerator time.
- Maximum energy available from accelerator. Some accelerators have maximum proton energies of 63 MeV, which may be too low for measuring saturation.
- Accuracy of error-rate prediction. An accurate prediction of SEU rates in space depends on how well the data can be fit with one of the standard functions describing the dependence of cross-section on proton energy. Section 6.8 will detail those functions. The dependence of SEU cross-section on energy for older devices was described by the 1-parameter Bendel equation, which requires only one data point. However, the 1-parameter Bendel equation was found to be inaccurate for modern devices, and was replaced with a 2-parameter equation, which requires testing at a minimum of two proton energies. One measurement should be done near threshold and the other near saturation. More recently, the Weibull equation and the error function have been used to fit the data. They have more adjustable parameters and so require more data points.
- The use of degraders to change beam energy raises the issue of straggle. Degraders are blocks of material through which the proton beam passes prior to striking the DUT. As they pass through the material, the protons lose energy by an amount that depends on the block's thickness and the material from which it is made. Section 5.14 discussed how to calculate the proton energy loss using SRIM2000. The problem with using degraders is an effect called "straggle", which is the spread in energy around the average energy of the proton beam after passing through a finite thickness of material. The energy loss is probabilistic in nature, which is why the spread increases as the thickness of the degrader increases. As long as the blocks are relatively thin and reduce the energy by only a small amount, the straggle can be ignored, particularly at high energies where the cross-section is saturated. However, if thick degraders are used to reduce the average beam energy to the threshold energy where the cross-section rises rapidly, straggle can lead to errors in the measurement of cross-section. For example, a copper degrader available at IUCF used to reduce proton energy from 192.3 MeV to 59.6 MeV produces a spread in energy of 3.6 MeV(FWHM). A choice of degraders should be available at the accelerator facility.
- Measurements to determine the threshold are complicated by the fact that the cross-section is small and large proton fluences are required for good statistics. Large proton fluences can cause TID damage that will destroy the part well before measurements with

good statistics are obtained.(See section In this case it is advisable first to do measurements at high proton energies and then at lower proton energies.

6.2.2 Proton Flux.

The proton flux should be selected based on two factors: 1) the time required to reach a specified fluence and 2) the expected error rate. Because of the significant cost involved for beam time, all fluxes should be chosen with an eye toward saving beam time. However, too high a proton flux could lead to the system being overwhelmed and not operating properly. In the case of SEL, inaccurate values of fluence could occur due to the time lag between when an event occurs and when the beam is switched off. Good practice suggests that an initial run be made, and the results used to adjust the flux for subsequent runs.

6.2.3 Proton Fluence.

The fluence used for a test is determined by error statistics. If the number of single events is N then the error in the measurement is given by $N^{0.5}$. For an error equal to 10%, $N^{0.5}/N$ must be equal to 1/10, which set N = 100. To satisfy this criterion, at least a hundred SEEs must be logged. (For a detailed discussion of statistical error, refer to an introductory book on statistics.) This is sometimes not possible near the SEE threshold where the cross-section is small and the device might be damaged as a result of proton-induced TID or DD before the required number of SEE have been logged. (Although frequently ignored, plots of SEE cross-section versus energy should include error bars.) If there are no events, then the maximum fluence to test to is determined by the mission requirements. If the requirements are not known, testing should stop either after a fluence of 10^{11} protons/cm^2 or after destruction of the part, which ever comes first.

6.3 Whether to Test.

Many attempts have been made to relate the LET threshold for SEUs induced by heavy ions with the energy threshold for SEUs induced by protons.[ROLL90],[PETE92] In fact, a simple equation has been developed:

$$A_b = L_{0.1} + 15$$

where A_b is the A parameter in the Bendel 1-parameter equation and $L_{0.1}$ is the LET value at which the cross-section is 1/10 of its saturated value. The Bendel A_b parameter is the proton energy threshold for proton reactions that produce upsets. Evidently, parts that have very low LET thresholds for ions will have proton thresholds around 15 MeV, and as the LET threshold increases so does the proton energy threshold. In theory, if the LET threshold has been determined, it is possible to use the above equation to obtain the upset rate from the Bendel A_b. In practice, however, this equation is based on a very crude approximation and should only be used as a rough guide and not as a justification for avoiding testing of one kind or another.

If a part has been tested with heavy ions and the threshold LET for SEUs found to be smaller than 15 MeV.cm^2/mg, the part is very likely to be sensitive to SEUs generated by protons. Some parts exhibit great sensitivity to heavy ions, having LET thresholds lower than 15 MeV.cm^2/mg, yet they have been shown to be insensitive to protons. This has been observed for the case of SEL. Nevertheless, if a part is suspected of being sensitive to SEL, it should be tested with protons. Proton-induced SEL was first observed in 1992.[NICH92],[ADAM92]

6.4 Effect of Packaging

Because high-energy protons will penetrate the covers of most devices without losing much energy, devices can be tested without having to remove the lid or plastic covering the part. For example, a 100 MeV proton has a penetration depth in aluminum of 3.7 cm. At low energies the

protons have a much smaller range. For example, the range of 20 MeV protons in an alloy such as iconel is less than 1 mm and the lid or plastic should be removed. The best approach is to use SRRIM2000 to calculate the range of protons with low energies in materials. If the energy loss is significant, it is advisable to remove the packaging if possible, or get an accurate measure of the thickness and use SRIM2000 to calculate the energy loss.

6.5 Beam Control

At UCD, control of the beam is passed on to the test engineer. To gain familiarity with the software controlling the beam, one should try a few "dry runs" with no parts exposed. Also, to avoid accumulating fluence when the DUT is not operating, the DUT should be turned on and operating properly before being exposed to the proton beam. For the same reason, the beam should be turned off before the DUT at the completion of the test.

6.6 Special Concerns for Devices

6.6.1 SRAMs and DRAMs (Multiple-Bit Upsets)

There is a possibility that high-energy protons will cause multiple-bit upsets (MBUs) in modern SRAMs and DRAMs. MBUs were not observed during proton testing of older memories. MBUs are characterized by the fact that they occur simultaneously and are adjacent to each other. One possible cause of MBUs is the diffusion of charge away from the interaction point. Another is that the proton could strike the control circuitry and cause lines of upsets. In either case, it is important to be able to distinguish MBUs from SEUs to obtain an accurate "event" rate. It is important to have a bit-map to determine the presence of MBUs. Alternatively, one could use a low flux and do frequent reads of the device to see whether more than one upset occurred and then analyze whether it was a MBU.

6.6.2 Optical Detectors

For most devices it is not necessary to change the angle of incidence when doing proton testing. Optocouplers and photodetectors are the exceptions. Their cross-sections should be measured as a function of angle of incidence to determine whether direct ionization by protons contributes. A large increase in the cross-section at high angles of incidence signifies the presence of SEEs caused by direct ionization.

6.6.3 Single Event Transients

Accurate SET testing is only possible if the same conditions are also used during testing as expected in space. For example, SETs in optocouplers are affected by the output load, which should be identical to the actual output load used in the application. [REED98] Furthermore, the SET cross-section enhancement at grazing angle of incidence due to direct ionization by high-energy protons is much less than for low-energy protons because low-energy protons have larger LETs. [REED98] The use of degraders that spread the proton energies should be avoided when looking for enhancement of the SET cross-section at grazing angle of incidence because it makes it more difficult to identify whether direct ionization plays a role. Because the transients induced by protons are likely to be smaller in amplitude than those induced by ions, it is important to make sure the trigger level of the detection equipment is properly set. In addition, for later analysis of SET pulse height vs width, all transients captured on the oscilloscope should be stored.

6.6.4 Power MOSFETs

Single-event burnout in power MOSFETS has been studied in great detail.[TITU96] SEB is triggered in an "off" power MOSFET. Charge deposited either by heavy ions or by proton-

induced recoils turns on a parasitic bipolar transistor that sets up a current between the source and the drain. Regenerative feedback leads to a high current state that can burn out the device. SEBs observed in space have been attributed to heavy ions, but more recently, protons have also caused SEBs in regions where the radiation environment is dominated by protons.[TITU98] Some parts seem to be more sensitive to proton-induced SEB while others are more sensitive to heavy-ion induced SEB. Special procedures are required for SEB testing in power MOSFETs, because once a device has exhibited burn-out it must be replaced. This procedure requires more time and a large supply of parts. To prevent damage, a resistor is often added between drain and power supply to limit the maximum drain/source current. This prevents the triggering of the high currents that lead to breakdown. Another possibility is to us a power supply whose current can be switched off immediately it reaches a high value. Although most devices are run at de-rated voltages, which reduce the possibility of SEBs, it is still necessary to find the voltages at which SEB is still a problem.

6.6.5 Stuck Bits in Memories (DRAMs and SRAMs)

Stuck bits in memories have also been treated by Marshall [MARS99]. A stuck bit, also called a hard error, is caused by the localized deposition of sufficient charge to produce interface states that shift the threshold voltage sufficiently far that the device can no longer switch. This is a localized TID effect. They were first observed in DRAMs in 1993 [OLDH93] and the following year in a 1-Mbit SRAM [POIV94]. In the past, most stuck bits were attributed to heavy ions. More recently, however, stuck bits have also been attributed to protons. While testing memories for SEEs with protons, one should monitor both the stuck bits and the leakage current for total dose damage. Following the observation of excessive leakage current or stuck bits, the part should be replaced because of TID damage.

6.6.6 Epitaxial Devices (including SOI) with Small Dimensions

In devices where the lateral dimensions are larger than the depth, the proton SEU cross-section may exhibit angular dependence, i.e. the cross-section increases with increasing angle of incidence.[REED95] The reason for this angular dependence is that the spallation reaction products are preferentially scattered in the forward direction. SOI devices may exhibit this effect. At normal incidence, the amount of collected charge is limited by the very thin silicon layer and may not be sufficient to produce a SEU. However, at non-normal incidence, the forward-scattered daughter particles will travel a longer distance through the silicon before reaching the underlying oxide layer. More deposited charge at finite angle means that the SEU cross-section is angular dependent and increases with increasing angle of incidence.

6.6.7 Latchup

Protons are known to induce latchup in certain circuits, particularly those based on CMOS technology. Therefore, when planning to test these types of devices, precautions should be taken to ensure that the device is not damaged due to latchup during testing. This can be done by limiting the current with the use of resistors or by setting a limit on the maximum supply current. Should a SEL occur, it would be necessary to cold reboot the system. If this is necessary, the beam should be turned off immediately and kept off during the rebooting stage to avoid accumulating fluence when no test is being performed. Also, for latchup testing the flux is usually kept very low to avoid the accumulation of dose between the time the latchup is detected and the beam is turned off. Once the device is again operating properly, the beam can be turned back on. Therefore, the current to the DUT must be monitored remotely and the rebooting accomplished either automatically or remotely. As the supply voltage used for state-of-the-art devices is reduced, theoretical predictions show that the threat of latchup decreases. It is nevertheless prudent to test devices for SEL with protons to confirm that they are latchup free.

6.6.8 Analog-to-Digital Converters

Testing analog-to-digital converters (ADCs) is usually done in the quasi-static mode in which a constant voltage is applied to the input and the digital output is monitored while the part is exposed to the beam. Because of inherent noise, it is usually necessary to mask off some of the least significant bits. The part is run with the beam off and bits are masked off until there are no more SEUs. Most proton accelerators generate significant electrical noise that will add to the inherent noise. Therefore, the masking should not be done in the laboratory prior to traveling to the proton test facility. Instead, masking should take place once the part is in position in front of the exit port, but with the beam block in place so there are no proton-induced SEUs. Many of the ADCs are manufactured using BICMOS technology in which the analog part is bipolar and the digital part is CMOS. If the CMOS part is not sensitive to proton-induced upsets and the bipolar part is, most of the SEUs will manifest themselves as small deviations around the expected output, i.e., most of the upsets will be in the least significant bits. It is therefore essential to minimize the noise while testing so that the effects on the least significant bits can be evaluated. In addition, advanced ADCs are very fast and will not function well with long cables. Therefore, the testing equipment must be located close to the ADC and should be shielded against damage by stray neutrons and protons.

6.7 Testing at Speed

Electronic devices such as logic circuits and opto-electronic devices such as a fiber optic data bus must be tested at the same speed as that used in space because the error rate cross-section has been shown to be frequency-dependent, i.e., the higher the speed, the greater is the error rate. If the part is operated at a speed lower than intended, an underestimation of the error rate will result. Therefore, the bandwidth of the test setup should be commensurate with the test speed needs and this precludes having the test equipment outside the vault. The test equipment must be placed in the vault and controlled via an Ethernet or other system that allows remote control.

6.8 Number of Devices Tested

The number of DUTs of the same kind that can be tested will depend on many factors, including their size (which determines how many can be tested at once), beam time available, budget and number of devices available. Frequently, one has to settle for testing a single device because of cost or availability of parts. Generally, 2 devices from the same manufacturer and lot would be acceptable for SEE testing, although 3 would be preferable. COTS devices, known to have a large variability in threshold energies, certainly require testing of more than one part.

6.9 Data Analysis

Proper data analysis is an important aspect of proton-induced SEE testing. Proton testing is required for predicting SEE errors rates in space and involves the measurement of the proton-induced SEE cross-section as a function of energy. Two different theoretical approaches have been used to calculate the energy dependence. The first approach is to perform a Monte Carlo calculation (such as CUPID), which will not be discussed here. The second is a semi-empirical approach based on the energetics of nuclear interactions. There are three different equations that one can use for fitting the data - the Bendel 1-parameter equation, the Bendel 2-parameter equation and the Weibull equation. The Bendel 1-parameter equation is not as accurate and is no longer used, particularly if data is available at more than one proton energy.

6.9.1 Bendel 1-parameter Equation

The SEU rate was measured at a single energy and the value fit using the Bendel one-parameter function[BEND83], given by:

$$\sigma = (24/A)^{14}[1-\exp(-0.18Y^{0.5})]^4 \quad \ldots\ldots(1)$$

with $Y=(18/A)^{0.5}(E-A)$, and where E and A are in MeV. The cross-section is given in terms of upsets per proton per cm^2 per bit. If the SEU cross-section is to be measured at only a single energy, 60 MeV would be a good choice for a lightly shielded device, because there are generally as many protons in space with energies below 60 MeV as above.

6.9.2 Bendel 2-parameter Equation

Modifications to the Bendel one-parameter function involved using two fitting parameters to obtain better agreement.[SHIM89] The resulting two-parameter function is given by:

$$\sigma = S\,[1-\exp(-0.18Y^{0.5})]^4 \quad \ldots\ldots(2)$$

where S is the proton limiting cross-section and Y is the same as in the 1-parameter Bendel equation. Figure 6.4 shows a comparison of 1-parameter and 2-parameter fits to data for actual devices.[PETE97] The curves have the same cross section at 60 MeV but a good fit to the data is clearly obtained with only 1 curve. In general, it is better to use the 2-parameter rather than the 1-parameter equation.

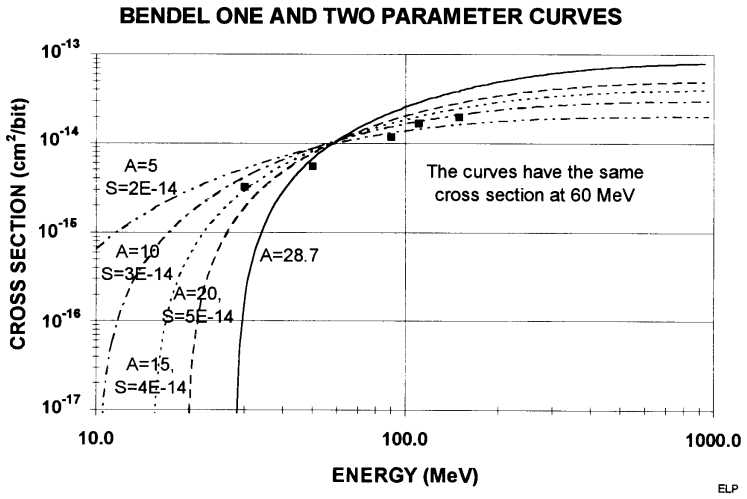

Fig. 6.4. Results of attempts to fit the proton SEU data with both 1-parameter and 2-parameter Bendel curves.

6.9.3 Weibull 4-parameter Equation

The integral Weibull function can also be used to fit the data and is given by:

$$\sigma = \sigma(\infty)[1-\exp(-((E-E_0)/W)^s] \quad \ldots\ldots(3)$$

where $\sigma(\infty)$ is the saturated cross-section, E_0 is the threshold energy, W is the width of the rising portion of the curve and S is the power that determines the shape. Because there are four variables in the Weibull function, a minimum of four different energy measurements must be made, particularly in the vicinity of the threshold where the cross-sections tend to be small. This approach is limited by the cost of beam time and the possibility of damaging the DUT when cross-sections are measured at energies close to threshold where a large fluence is required to obtain a few SEEs. However, it does provide a more accurate fit.

6.9.4 Proton Energies

The Bendell and Weibull functions all have the same basic shape – a smoothed out step function that has a threshold at relatively low energy followed by a gradual rise to a saturated value at high energies. For the most accurate predictions, it is necessary to obtain the complete shape of the SEE cross-section curve as a function of energy. However, the two most important parameters are the threshold energy and the saturated cross-section. Most SEE cross-section curves resulting from proton testing are saturated at proton energies above 100 MeV. This involves a single measurement at energy greater than 100 MeV. In contrast, it generally requires more than one measurement to determine the threshold. For confirmation that the measurements agree with the theory, cross-sections could be measured at additional energies, but the actual number of energy values depends on budget and accelerator availability

6.9.5 Check on results

6.9.5.1 PROFIT

If heavy-ion SEU data is available, one can use PROFIT to check on the results. [CALV96] The equation is:

$$\sigma(p)_{sat} = \sigma(LET=15).c.N_{at}.\sigma_{nuclear} \qquad (4)$$

where $\sigma(p)_{sat}$ is the saturated proton cross-section, σ(LET=15) is the heavy-ion cross-section measured at LET = 15 MeV-cm^2/mg, c is the charge collection depth, N_{at} is the number of Si atoms per cm^3, and $\sigma_{nuclear}$ is the average nuclear cross-section (6x10^{-26} cm^2) for protons between 100 MeV and 200 MeV. However, the agreement is good in some cases and not so good in others, so care should be exercised when using this technique.

6.9.5.2 FIGURE OF MERIT

Another check on whether the measured proton cross-section is reasonable is to use the Figure of Merit (FOM) [PETE96]. The FOM for heavy ions is given by:

$$FOM = \frac{\sigma_{HL}}{L_{0.25}^2} \qquad (5)$$

where σ_{HL} is the limiting heavy-ion cross-section per bit at large LET and $L_{0.25}$ is the LET at 25% of the limiting cross-section. The FOM can also be obtained from the limiting proton SEU cross-section σ_{PL}:

$$FOM = 4.5 \ x \ 10^4 x \sigma_{PL} \qquad (6)$$

A check to see whether σ_{PL} is reasonable can be done by calculating the FOM from equation (6) and comparing it with the FOM calculated from equation (5) using the heavy-ion data. A large disagreement signals the possibility of an error in the one or both of the measurements.

7.0 TID Issues and Lessons Learned

The basic message of this section is that using a proton beam to test for TID is rarely cost-effective due to annealing, enhanced low dose rate effects and the need to test multiple devices. Most TID testing is accomplished with gamma rays in a ^{60}Co cell. However, because TID effects often occur in conjunction with SEE and DDD, it is important to understand the mechanisms responsible for TID so that in those cases where, for example, both SEE and TID need to be measured, they can be done simultaneously with protons.

7.1 Background

In the previous section we discussed the effects of free-carrier generation in semiconductors. In this section we will discuss free-carrier generation by ions in insulators, such as oxides used in integrated circuits. The ions generate tracks of e-h pairs in insulators that can lead to device degradation or failure via TID. Many years of research devoted to the study of radiation effects in the most common insulator SiO_2 have resulted in a good understanding of the mechanisms involved. Not all aspects, however, are understood and the research continues apace. Previous short courses at the annual Nuclear and Space Radiation Effects Conferences provide excellent and detailed discussions of TID effects. [FLEE95], [DRES98], [LERA99]

As already pointed out, proton beams are not the first choice for doing TID testing because of cost, beam availability, and dose rate effects. Most radiation test engineers use X-rays from an X-ray generator or gamma rays in a Co^{60} cell to test for TID. Both X-rays and gamma rays are high-energy photons that produce radiation damage via ionization of the atoms making up the oxide. Even though photons are very different from protons, the concept of absorbed dose to describe energy loss applies to both and depends on LET. In fact, data suggests that there is very little difference between a rad(SiO_2) generated by protons or by photons.[PEAS01]

There are, however, differences in charge generation in Si and SiO_2. One difference is the amount of energy needed to generate an e-h pair in Si (3.6 eV on average) compared with SiO_2 (17 eV). Another difference is the much lower carrier mobilities in SiO_2 compared with Si; the electron mobility is 20 $cm^2V^{-1}s^{-1}$ and hole mobilities range from 10^{-4} to 10^{-11} $cm^2V^{-1}s^{-1}$, depending on electric field and temperature. A model that has proved useful for describing hole mobility is that of polaron hopping via the continuous random walk approximation.[MCLE76] In the presence of an electric field, the electrons rapidly exit the oxide, while the holes move much more slowly in the opposite direction, hopping from one site to another. The larger the electric field and the higher the temperature, the faster the holes move. For positive bias on the gate of a MOSFET, electrons in the insulator move towards the gate and holes move towards the interface between the insulator and the semiconductor. Some of the holes become trapped in the vicinity of the interface where they form a layer of positive charge. The electrical characteristics of transistors are altered by the presence of charge in the vicinity of the interface. As an example, trapped positive charge shifts the threshold voltage of MOS transistors. In addition, by a process that is not completely clear, the holes also lead to the formation of interface traps that also affect transistor performance through threshold voltage shift and majority carrier mobility degradation.

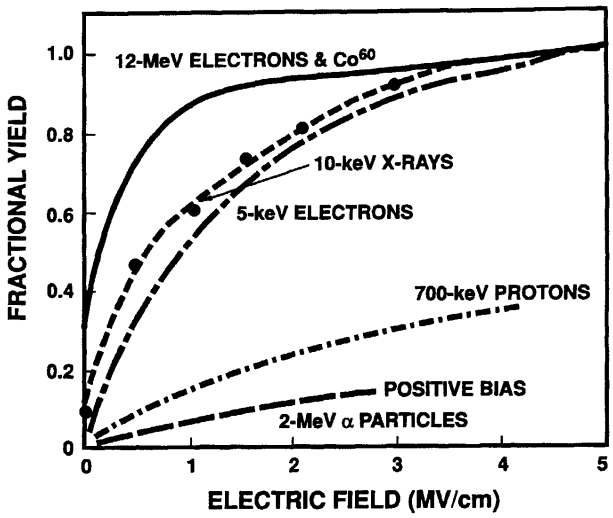

Fig. 7.1. Fractional yield of charge generated by various forms of radiation as a function of electric field.[MCLE89]

Recombination of e-h pairs plays a big role in determining how much damage results from a specific dose. The greater the recombination, the fewer holes remain to produce trapped charge and interface states. Geminate recombination, in which the e-h pair recombines with itself, occurs for low e-h densities generated by low LET ions or gamma rays.[AUSM86] Columnar recombination refers to electrons and holes recombining with other holes and electrons and dominates at high e-h densities generated by high LET ions.[JAFF13] Therefore, geminate recombination will dominate for high-energy protons with low LETs and columnar recombination will dominate for low energy protons with higher LETs. At intermediate LETs, both geminate and columnar recombination will contribute. Recombination is suppressed in the presence of an electric field resulting in a larger fractional yield of carriers in the oxide. Fig. 7.1 shows a large variation in the fractional yield of carriers for different kinds of radiation.[MCLE89] For example, under an electric field of 2MV/cm, the fractional yield for exposure to ^{60}Co gamma rays is over 90%, whereas that for 700 keV protons is about 25%. High-energy protons should have a higher fractional yield than low-energy protons.

The trapped positive charge gives rise to an electric field that shifts the transistor's threshold voltage in the negative direction. For example, in an n-channel MOS transistor operating in inversion, the trapped holes tend to make it harder to turn the device off.[FLEE95] The holes also produce interface states via processes that are not fully understood, but are known to depend on temperature, electric field, time and total dose. The interface states have energies that cover most of the semiconductor energy bandgap. Those above the Fermi level are acceptors and those below are donors. Therefore, for both n- and p-channel MOS transistors, the absolute value of the threshold voltage increases after irradiation due to the creation of new interface states. TID damage may manifest itself as an increase in the leakage current, a change in the frequency response, and, ultimately a total loss of functionality.

The magnitude of TID damage depends on exposure rate (proton flux) and elapsed time following exposure. Such time-dependent effects occur because the holes move relatively slowly towards the interface and, once trapped, they can be annealed out over time, especially at elevated temperatures. A detailed discussion of time dependent effects is beyond the scope of this report and the interested reader is referred instead to a number of excellent articles that include

discussions of time-dependent effects.[DRES98], [MCLE89], [FLEE95] A brief description of the manifestations of dose-rate effects and annealing is in order.

One important time-dependent effect that poses problems for proton TID testing is known as enhanced low dose rate sensitivity (ELDRS) in which certain bipolar devices have been shown to degrade at much lower levels of TID if the dose rate is well below 1 rad(Si)/s, a dose rate more akin to that in space.[NOWL92] Fig. 7.2 shows an example of how the level of damage depends on dose rate. To test a device to a TID level of 1 krad(Si) at a dose rate of 0.01 rads(Si)/s would require about 30 hours. Because of beam costs and availability and because of difficulties related to controlling a beam with such low flux, this is clearly not a practical method of doing low dose-rate testing. Therefore, proton beams should never be used for ELDRS testing.

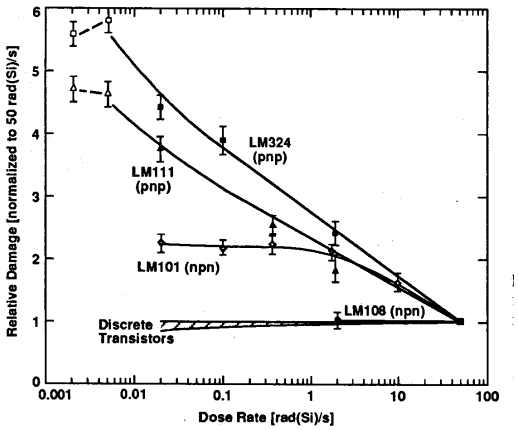

Fig. 7.2. Relative damage as a function of dose rate for various linear devices.[JOHN94]

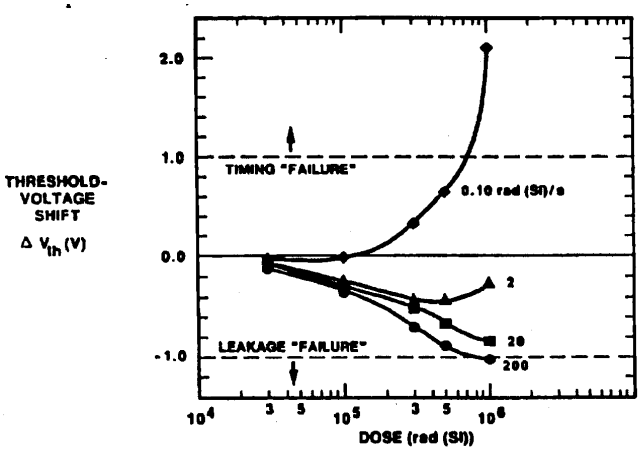

Fig. 7.3. Threshold voltage shift as a function of dose for different dose rates, illustrating how the different time constants for trapped charge and interface state generation and anneal affect the magnitude of the threshold voltage shift.[WINO86]

Another dramatic example of a dose-rate effect that has been known for some time is "super-recovery" or "rebound".[WINO86],[FLEE95] Super-recovery refers to the fact that, while the initial trapped positive charge begins to decline due to annealing, the interface state density continues to increase. As was previously pointed out, irradiation produces both trapped positive charge and interface states. Fig 7.3 shows that at low dose rate, the threshold voltage shift is positive and the part fails due to timing problems, whereas at high dose rates the part fails due to a negative threshold voltage shift that results in a large leakage current. The positive charge is trapped in a much shorter time than required for the buildup of interface states. In addition, the positive charge can undergo annealing, whereas the interface states do not. Therefore, n-MOS transistors irradiated at high dose rates (>50 krad(Si)/s) will exhibit a buildup of positive charge that shifts the threshold voltage in the negative direction leading to failure through excessive current leakage. Over short time intervals, the buildup of interface states is negligible so they do not contribute. However, if the n-MOS device is irradiated at low dose rate (< 1 rad(Si)/s), the positive charge has time to anneal, reducing the amount of negative voltage shift. At the same time, the negative interface states have an opportunity to grow, causing a positive shift in the threshold voltage. The combination of the two can lead to such a large positive shift that the device will fail through timing effects. Test Method 1019.5 addresses these issues by requiring high-temperature annealing following high dose-rate testing. Therefore, in principle, devices can be tested for TID using proton beams if Test Method 1019.5 is followed. However, it is still an expensive alternative to ^{60}Co testing because of the need to test multiple parts, especially COTS parts that are known to have large variability in failure levels.

On occasion the test engineer wishes to test parts after incremental steps of TID to monitor how the part's functionality or other parameters change with dose. After each TID increment, the parts have to be tested and this can consume a great deal of time, adding significantly to the cost of testing. In this case the advantage of using ^{60}Co is clear.

Exposure of devices to proton beams produces both TID and DD damage. However, majority-carrier devices, such as those based on MOS technology, are not affected by DD. Therefore, it is not necessary to test MOS devices for TID damage using proton beams. Instead they should be TID tested using ^{60}Co or X-ray sources. The only reason to consider TID testing at a proton accelerator is if it is done in conjunction with other measurements, such as during SEE or DD testing. For instance, testing a CMOS memory for SEUs with a proton beam will also result in TID damage. After significant exposure, as would be the case in a SEU hard device, the TID damage may be so severe that the device exhibits increased leakage current, stuck bits, and, in the worst case, failure to operate. It is important to know the levels of TID damage when doing SEE testing because the TID damage can skew the SEE data.

Certain devices, such as optocouplers, degrade via both TID and DD with the DD contribution overwhelming that of TID. Testing optocouplers with ^{60}Co or X-rays alone will grossly understate the damage levels because these two techniques do not generate significant DD. Therefore, optoelectronic devices that degrade via both TID and DD should be tested with proton beams for a more realistic assessment of their survival levels in a proton-dominated environment.

7.2 Calculation of Total Ionizing Dose

The TID from protons can be calculated from the proton LET and the fluence by using the following formula:

$$\text{Dose}(\text{rads}(SiO_2)) = (\text{LET}(SiO_2)) \bullet (\text{Fluence}) \bullet (1.6\text{E-}05) \quad \ldots\ldots\ldots\ldots\ldots\ldots\ldots\ldots (7)$$

The LET, which has units of MeV-cm^2/mg, is obtained from SRIM2000 with proton energy and SiO_2 as inputs. The fluence (#/cm^2) is obtained from the computer controlling the exposure. As an example, a 60 MeV proton has a LET of $9x10^{-3}$ MeV-cm^2/mg in SiO_2 so that a TID of 100 krads(Si) will require a fluence of approximately $7x10^{11}$ particles/cm^2. The accelerator at UCD produces a beam with a diameter of 6 cm, which is equivalent to an area of approximately 27 cm^2. Using a beam current of 1 nA, the TID of 100 krad(Si) can be accumulated in approximately 1 hour. Test Method 1019 specifies the dose rates required for doing TID testing to take into account effects such as "rebound." Although Test Method 1019 only applies to gamma ray testing, it can, nevertheless, be used as a guide for selecting the proton flux (dose rate) when doing TID testing with protons.

7.3 Factors Affecting TID Damage

Ideally one would like a one-to-one correspondence between dose deposited and damage. Factors that affect this one-to-one correspondence are the density of e-h pairs generated by the protons (which depends on proton energy) and the magnitude of the electric field in the oxide. These two factors affect the rate of recombination, which ultimately determines the damage level. Therefore, the proper proton energy should be selected and the device should be under the appropriate bias during testing.

7.3.1 Proton Energy

The choice of proton energy needed for TID testing depends on the space environment and on shielding. As pointed out in the introduction, the number of holes that survive long enough to reach the interface is affected by either geminate or columnar recombination. High-energy protons have low LETs which lead to low-density charge tracks for which geminate recombination dominates. Conversely, low-energy protons have relatively higher LETs producing higher density tracks for which columnar recombination dominates. An additional factor suppressing columnar recombination is the electric field itself. Therefore, if there is sufficient shielding to reduce the flux of electrons and low-energy protons, the particle spectrum seen by the DUT will be dominated by high-energy protons. This suggests that TID testing be done with high-energy protons (> 60 MeV). Furthermore, TID testing with protons should also be done under the proper operating biases because they affect the recombination. If the spacecraft does not provide much shielding, low-energy protons and electrons will dominate the environment seen by the DUT. This is a more complicated situation because electrons produce low density tracks for which geminate recombination dominates, whereas low-energy protons produce relatively higher density tracks for which columnar recombination dominates. For the case where the electron flux exceeds the proton flux, high-energy protons may be used for TID testing. When the proton flux is greater, low-energy protons should be used.

7.3.2 Testing Under Bias

Because bias is, in most cases, the condition that leads to the most severe TID degradation, proton testing should be done under the bias expected when the part operates in space. Fig. 7.1 shows charge yield as a function of electric field. Evidently, the charge yield is greatly reduced in the absence of bias suggesting that the parts should always be tested under bias. The most realistic conditions involve testing the part under the bias applied during normal operation.

7.4 Selection of Proton Flux

The proton flux determines the dose rate. For the case of gamma irradiation, it is specified by MIL Std 883 Test Method 1019. This test method suggests a range of dose rates from 50 rads(Si)/s to 300 rads(Si)/s. Although test method 1019 does not include proton testing, it can be

used as a guide for selecting dose rate. The proton dose rate can be calculated using the equation given in Section 7.2. Accelerators have no difficulty supplying proton fluxes that give dose rates in the range specified by Test Method 1019. The reason for not doing TID testing with protons becomes evident when post irradiation effects (PIE) are considered. As an example, consider TID testing for MOS devices. Test Method 1019 specifies that following irradiation, a room temperature anneal should be done until parametric values return to within specifications, but no longer than the time the device will be exposed to radiation in space. This essentially means that only one exposure can be done and then the device must be returned to the test engineer's laboratory for the annealing part which may take many weeks. Accelerated annealing is another option and involves first exposing the devices to 1.5 times the intended application specification and then heating it at 100 ^{o}C for 168 hours. This is clearly even less practical for testing at a remote proton accelerator. A greater difficulty arises when testing certain bipolar circuits for enhanced low dose rate sensitivity (ELDRS), which is not addressed in MIL STD 883 Test Method 1019. For ELDRS, one needs dose-rates of around 0.01 rad(Si) per second. Such a low dose-rate is not practical with a proton beam, because of beam time costs and availability. Very high fluxes may distort the internal electric fields in the oxides due to the creation of charge that screens out the electric field. At sufficiently high fluxes, the DUTs temperature might rise due proton energy absorption.

7.5 Estimate of TID Levels before Testing.

A TID test usually involves a series of radiation exposures followed by measurements to determine functionality or the value of some device parameter sensitive to TID. To decide on what dose increments to use requires a rough idea of the dose at which the device fails. The number of increments is limited by the accelerator time available. As an example, if it is suspected that the device fails at 10 krad(Si), one might choose to test at the following TID levels: 1 krad(Si), 2 krad(Si), 5 krad(Si) and 10 krad(Si). A totally different set of TID levels would be used if the part were known to have a failure level of 100 krad(Si). They might be 10 krad(Si), 20 krad(Si), 50 krad(Si) and 100 krad(Si). Selecting the latter levels to test a device that actually fails at a TID level of 10 krad(Si) would not provide the necessary data. Obviously, it is not always possible to know the DUT's failure level ahead of testing. Sometime an educated guess can be made based on known TID levels of similar parts in the same technology.

7.6 Monitoring TID Damage

TID damage manifests itself as either a change in a particular operating parameter, such as leakage current, or as a failure of the device to function. Therefore, if TID is expected to occur when testing for SEE, the proper device parameter must be monitored. A TID screening test using gamma rays in a ^{60}Co cell should be done before SEE testing to see whether it will survive the expected TID levels. If it will not survive, then one can save a considerable amount of money by not doing any SEE testing.

7.7 Testing More than One Device

If the devices are much smaller than the beam diameter and more than one device needs to be tested, it is recommended that more than one device at a time be positioned in the beam and tested. The size of the beam and the uniformity vary from one accelerator to another. This will limit the number of samples that can be tested at a time.

7.8 Fluence and TID

If the part being tested for SEE is not very sensitive and if the proton energy is near the threshold, there are likely to be very few SEEs. Obtaining decent statistics requires a high fluence at relatively low proton energies which means the TID might limit the testing. However, the high fluences might cause TID failure. Consider a part that has a TID failure level of 10

krad(Si) when exposed to 30 MeV protons. For a fluence of 1 proton/cm^2, the dose is $3x10^{-7}$ rads(Si). After a fluence of $3.0x10^{11}$ particles per cm^2, the device will fail. At 30 MeV, the cross-section might be quite small – on the order of 10^{-10} cm^2. For good statistics at least 10 upsets are needed, which means that we must expose the part to 10^{11} protons/cm^2. This means that the dose is $3.0x10^4$ particles/cm^2, which is 30 krad(Si) and many parts will fail before reaching that level.

7.9 Dose Modified by Shielding.

To calculate how shielding modifies the absorbed dose, one can use the computer program SHIELDOSE[SELT80] The program calculates the absorbed dose as a function of depth in aluminum shielding material of spacecraft, imparted by electrons and protons in orbit. SHIELDOSE calculates, for arbitrary proton and electron incident spectra, the dose absorbed in small volumes of different detector materials for the following aluminum shield geometries:

- a semi-infinite plane medium, as a function of depth; irradiation is from one side only,
- at the transmission surface of a plane slab, as a function of slab thickness; irradiation is from one side only.
- at the centre of a solid sphere, as a function of sphere radius; irradiation is from all directions.

The program is part of SPENVIS (*www.spenvis.oma.be/spenvis*) and can be used for a first approximation of the absorbed dose. For doing more refined calculations in three dimensions, a powerful program is NOVICE.

8.0 Displacement Damage Dose Testing

So far, this monograph has dealt with two of the three types of radiation damage produced by protons – SEE and TID. The third type involves the degradation of electric or optical performance as a result of proton-induced displacement damage (DD) that occurs in a wide range of devices, including bipolar transistors, light emitting diodes and photodetectors. Although DD occurs everywhere in an integrated circuit, only DD in the semiconductor degrades. This differs from TID, which occurs in insulators used in the construction of transistors. Devices, suspected of exhibiting DD sensitivity, should be tested for their level of sensitivity if they are to operate in proton-rich environments, such as in the belts around the earth.

8.1 Background

Both SEE and TID damage in devices operating in space are caused by ions losing energy via ionization of the material they pass through. Ions also lose energy via another mechanism - non-ionizing energy loss (NIEL) - a process whereby the incident ions collide both elastically and inelastically with atomic nuclei, knocking them out of their equilibrium positions in the process. The atomic nuclei initially displaced by the incident ions are called primary knock-on atoms (PKAs). The damage associated with displaced atoms in the semiconductor lattice is called displacement damage (DD) and the equivalent dose is termed displacement damage dose (DDD), a concept that has not yet been widely accepted. Although less than 0.1% of the total energy lost by a proton is via NIEL, DD effects can cause significant performance changes in device such as optocouplers, LEDs and CCDs. The reader is referred to the following three excellent review articles on DD. [MARS99], [SUMM92], [SROU88]

The interstitials and vacancies, produced as a result of nuclear collisions, form Frenkel pairs. Most of them recombine within a very short time (~ 1 sec) and no permanent damage is produced. A few of the Frenkel pairs escape recombination and form stable defects. One component of a Frenkel pair, the interstitial atom, is electrically inactive and has no effect on device performance, especially for very high energy (>100 MeV) irradiations. The other component, the vacancy, may form many different types of electrically active complexes. For example, the vacancy may combine either another vacancy to produce a divacancy, or with a dopant atom (phosphorus or oxygen) to form an electrically active defect. The defect density depends on the recoil energy of the PKA. At low recoil energy (< 2 keV), coulomb scattering dominates and numerous isolated defects are produced. At high recoil energy the interaction cross-section is lower, but the defect structure is more complicated, taking the form of cascades or tree-like structures that contribute a significant fraction of the total DD. [WOOD81].

The vacancy complexes are crystal lattice defects with energy levels (traps and generation/recombination centers) in the semiconductor bandgap. As such, they can have a major effect on device performance. The most important material parameters governing the operation of semiconductor devices are minority carrier lifetime (recombination lifetime), generation lifetime, majority carrier concentration and majority carrier mobility. [MARS99] Energy levels in the semiconductor bandgap associated with DD are capable of affecting any one of these material parameters. In general, the generation and recombination centers have an order of magnitude lower density than the majority carrier concentration. Therefore, the minority carrier lifetime, which depends on the density of generation and recombination centers, will be degraded well before the carrier concentration. Since mobility degradation is not significant, except at very high damage levels, DD will have the most effect on devices that depend on minority carrier lifetimes through generation and recombination. Minority-carrier lifetime degradation causes reductions in the gain of bipolar transistors, the responsivity of detectors and the efficiency of solar cells. Certain light sources, such as amphoterically doped LEDs, are greatly affected by DD, whereas others, such as lasers, are not. The reasons for these differences are not yet well

understood. DD has very little effect on MOS-based devices, in part because the operation of MOS devices is governed by majority carriers rather than by minority carriers, and because of the relatively small amount of energy lost by NIEL compared with the amount lost by ionization. Therefore, TID effects will appear in MOS devices well before any effects due to DD.

Laboratory sources of radiation used for TID testing, such as X-ray generators and ^{60}Co do produce some DD, but they are generally not used for DD testing because they produce only relatively small amounts of DD. Instead, DD testing is done with protons or neutrons. Proton testing is usually done at accelerators, such as cyclotrons, whereas neutron testing is done either at a reactor, such as the one at Aberdeen Arsenal, or at an accelerator, such as the one at Los Alamos National Laboratory. Neutrons are produced in an accelerator when high-energy protons collide with heavy nuclei, such as lead, in thin foils placed in the proton beam. It has been demonstrated experimentally that some devices, such as CCDs, optocouplers and solar cells, degrade via both DD and TID. Combined effects are usually tested with protons, which are capable of producing both TID and DD, rather than neutrons, which produce primarily DD. In cases where it is necessary to study DD effects without the complications of TID, neutrons from accelerators are used. High-energy (>1MeV) electrons may also be used for generating DD. Although electrons, like protons, lose most of their energy via ionization, they do produce defects, albeit only isolated defects. To generate defect clusters, high-energy protons are needed.

The amount of DD produced by protons depends on their energy – the lower the proton energy the greater is the DD density. Protons in space have a wide range of energies, which requires that the DD must be known for the whole range of proton energies if accurate predictions of total DD are needed. To avoid having to measure DD over a wide range of proton energies, testing is done at a few energies and the full damage spectrum is obtained from NIEL calculations. Either analytical or Monte Carlo methods may be used to calculate NIEL. The analytical calculation is quite complicated and the interested reader is referred to the following references.[BURK86],[LIND63] Large differences in energy loss rate for NIEL and for ionization are shown in figure 8.1. The Monte Carlo programs for calculating NIEL are HETC, CUPID and SRIM. The reader is warned against using TRIM for calculating NIEL for protons with energies greater than 8 MeV because TRIM includes only elastic (Coulombic) interactions that dominate for proton energies less than 8 MeV. At energies greater than 8 MeV inelastic processes dominate and these are not included in TRIM. Were TRIM to be used for calculating NIEL for high-energy protons, an underestimation of the total DD would result. This underscores the importance of including the proton energy spectrum in calculations of NIEL. NIEL is to DD what LET is to SEE and TID, and even has the same units (keV•cm^2/g).

The environment experienced by a device in space also has a neutron component produced when cosmic rays interact with matter, such as spacecraft shielding. The thicker the spacecraft shielding, the greater is the flux of secondary neutrons. For example, secondary neutrons may constitute a significant fraction (10%) of the proton fluence when the shielding consists of 0.2 cm thick tungsten. [JUN01] Neutrons are also produced when cosmic rays interact with nitrogen atoms in the earth's atmosphere. Although they are capable of producing SEUs in dense memories on board aircraft flying at high altitudes (60,000 feet) and high latitudes, their flux is not sufficient to produce significant DD.[TABE93]

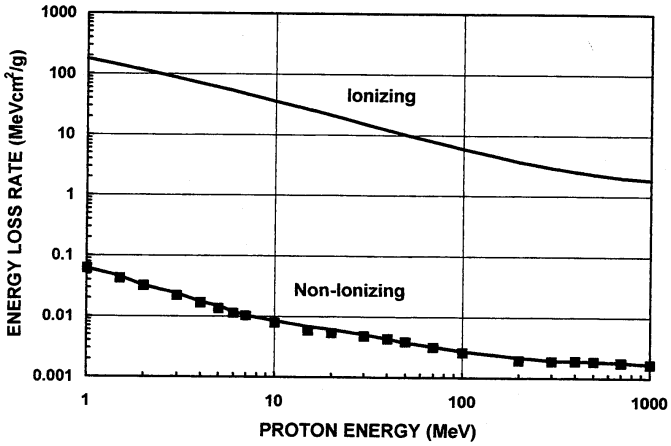

Fig. 8.1. Energy loss calculations for protons in silicon via both ionizing and non-ionizing mechanisms.[MARS99]

The next step after calculating NIEL is to make the connection between NIEL and device performance degradation. Damage caused by NIEL can affect material parameters that are dependent on the density of generation/recombination centers. One such example would be the reduction in the diffusion length (L) with fluence (Φ) according to the following equation:

$$1/L^2 = 1/L_o^2 + K\Phi$$

The factor K denotes a "*damage constant*" that can be calculated if L, L_o and Φ are known. However, this is not very useful because material parameters cannot, in most cases, be measured. Instead, test engineers measure device or system parameters, such as bipolar transistor gain, solar cell efficiency or photodiode dark current. These parameters are measured as a function of fluence, and most of them (but not all) are linearly dependent on fluence. For instance, the change in the inverse of bipolar transistor gain is related to the fluence through a "*damage factor*" according to the following equation:

$$1/h_{FE} = 1/h_{FE0} + K(E, \text{particle type})\Phi$$

Here, the factor K(E, particle type) is the particle and energy dependent displacement damage factor, which is determined by measuring the transistor gain both before and after exposure to a proton fluence, Φ. This kind of equation holds for other device parameters, such as solar cell efficiency and dark current, and for different energies and particle types. (One exception is the empirical equation for solar cell power, which exhibits a logarithmic rather than simple linear dependence.)

The final step is to relate the damage factor (K(E, particle type)) to NIEL. It has been shown empirically that, for most devices, the damage factor depends linearly on NIEL, i.e.,

$$K(E, \text{particle type}) = C \bullet NIEL(E, \text{particle type})$$

This relationship is demonstrated empirically for the minority carrier lifetime in a bipolar transistor. Fig. 8.2 shows the minority carrier lifetime damage factor ratio as a function of proton energy and particle type for a number of different transistors. K(E, particle type) is calculated from the data for each transistor, energy and particle type. The data are normalized to that calculated for damage in Si induced by 1 MeV neutrons. Then NIEL calculations are carried out

and the results are also normalized to the NIEL for 1 MeV neutron-damage in Si. Fig. 8.2 shows the data points in the energy range from 4 MeV to 200 MeV and for protons, deuterons and helium ions. The calculated NIEL ratios for the energy and particle of interest normalized to 1 MeV neutron-damage are shown as the solid lines. The figure shows that the data points match well with the calculations and no scaling factor is needed to relate the device performance degradation to the NIEL. This comparison has been made for a number of different device parameters and, in most cases, exhibits a linear relationship.

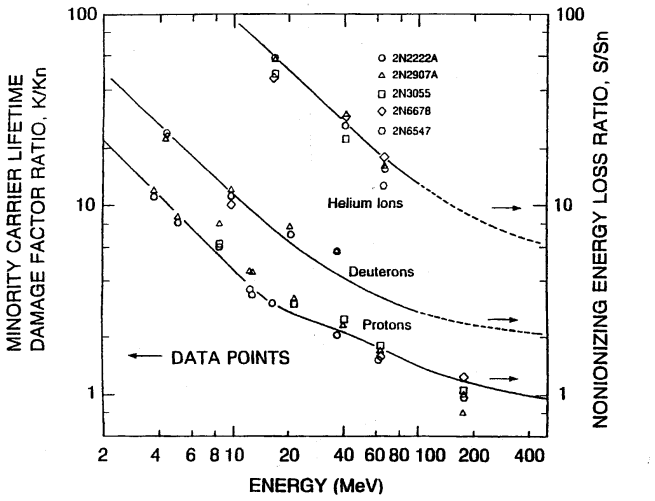

Fig. 8.2. Dependence on proton energy of minority carrier lifetime damage factors and NIEL.[SUMM87]

It is essential, when performing NIEL calculations, to be aware of the following limitations:

- In general, NIEL calculations for Si devices are fairly accurate, giving results within a factor of two of the measured values. However, there are discrepancies at both low (<20 eV) and high energies (>20 MeV) so that if NIEL is calculated at either the low or high energy limits and the result scaled to all other energies, the total NIEL curve will be significantly in error.
- NIEL calculations at very low proton energies (a few eV) close to the displacement damage threshold in Si, are known to be inaccurate and measurements at those energies should be avoided. [DALE88] A complicating factor for low-energy protons is that the NIEL changes along the proton's path as it slows down and comes to a stop.
- There are also discrepancies at high proton energies. Discrepancies between measured damage factors and those calculated from NIEL have been noted in GaAs devices.[BARR95] This area is currently under active investigation and promising progress has recently been reported, which should lead to more accurate NIEL measurements for high-energy protons.[MESS01, WALT01].
- A questionable assumption affecting the calculation of NIEL is that the displacement damage factor is always linearly dependent on NIEL. In some cases, the dependence has been shown to be super-linear, with more damage at higher NIEL or lower proton energy.[DALE89] Theories have been proposed to explain this effect. One theory attributes the effect to the dependence of the PKA energy spectrum on proton energy and the fact that Frenkel pairs produced by low-energy PKAs would have lower recombination rates, with a concomitant higher damage factor.[DALE93]

- Another assumption that does not always hold is the linearity between the degradation of the device parameter of interest and the fluence. This is clearly seen for devices such as optocouplers where:

$$1/CTR_f \neq 1/CTR_i + K\Phi$$

CTR_i is the initial current transfer ratio, defined as the detector current divided by the LED current, CTR_f is the current transfer ratio after irradiation, and Φ is the fluence. The analysis of this case is more complicated because optocouplers consists of three components, LEDs, photodetectors and coupling media, and the CTR depends on both TID and DD. This is discussed in more detail in section 9.1.

The concept of "damage equivalent fluence" is frequently used when comparing DD produced by any particle having any arbitrary energy. The concept refers to the fact that the particle fluences required to produce a specific level of DD in a device for two different particles having different energies can be compared using NIEL. As a consequence, measurements of the damage factor as a function of fluence for a particular particle at a single energy makes it possible to predict the level of damage at any energy and for any other particle. This effectively limits the required amount of accelerator testing, thereby saving money and time. This approach is based on accurate knowledge of the energy dependence of NIEL, which is not always the case. The reduced energy range limits the uncertainty in the NIEL calculations and requires careful selection of proton test energy.

The differential proton fluence spectrum to which a shielded device is exposed in space is a continuum in energy, the exact shape of which depends on the environment and on the shielding material and thickness. Instead of having to take data at a large number of different energies, data at a few energies should suffice. Then, assuming that the damage factor depends linearly on NIEL, the change in a device parameter can be predicted for any particle fluence at any energy. By extension, the DD for a particular proton spectrum involving a continuum of energies can be determined. This information is needed for the calculation of the total DD in a device exposed to protons with a broad energy spectrum.

8.2 Proton Energy

Because of cost and time, proton DD testing should be done at only a few proton energies, possibly just one or two energies. Selection of the optimum proton energy for DD testing depends on the DUT's anticipated environment, consisting of the natural radiation environment modified by shielding. Unshielded devices (e.g. solar cells) may experience a significant amount of DD from electrons and low-energy protons, whereas well-shielded devices will experience relatively more damage from high-energy protons (40-100 MeV). Although the damage, as measured by the electrical characteristics, may appear to be the same at high and low proton energies, there are important differences in such factors as the rate of annealing that mandate a more careful selection of energy.

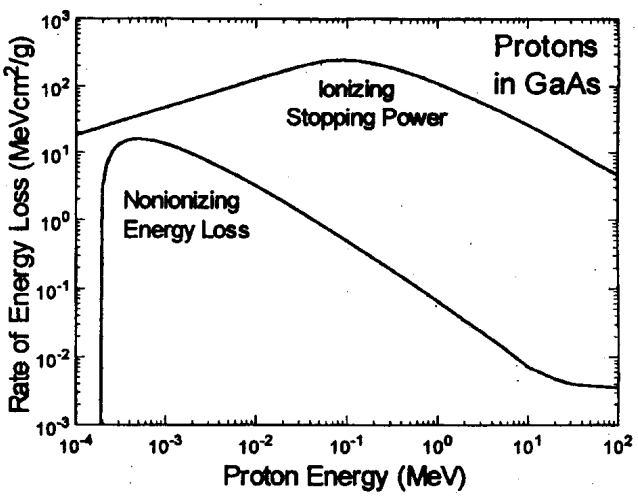

Fig. 8.3. Rate of energy loss in GaAs as a function of proton energy for both ionizing and NIEL.[MESS97]

One criterion suggested for selecting proton energy is based on the NIEL-weighted proton energy spectrum, which is obtained by convoluting the calculated NIEL dependence on proton energy with the proton energy spectrum modified by the proton's passage through shielding.[MARS99] Therefore, knowledge of both the NIEL dependence on energy and the shielded proton spectrum are needed. Fig. 8.3 shows the energy loss due to both ionizing and non-ionizing (NIEL) interactions in GaAs. There is a very sharp onset of the NIEL curve at 200 keV and a maximum at about 300 keV. By about 10 MeV, the rate of energy loss via DD is down by more than three orders of magnitude. (The NIEL spectrum for protons in silicon is qualitatively similar.) The proton energy spectrum at the device depends not only on the location of the spacecraft and on the time, i.e., whether the spacecraft is exposed to a solar proton event, but also on the degree of shielding. Heavily shielded devices will be exposed to relatively few low-energy protons and the displacement damage testing can be done at energies of around 50 MeV, close to the NIEL weighted maximum. On the other hand, lightly shielded devices, like solar cells, will be exposed to more low-energy protons and the maximum in the NIEL weighted proton spectrum will shift to lower energies.

Fig. 8.4 shows a comparison of the cumulative fraction of ionizing and displacement damage dose in GaAs as a function of slowed-down proton energy for a solar proton event such as that of 19th October 1989.[MESS97] The figure clearly shows that a significant portion of the total displacement damage for a lightly shielded device (3 mils SiO_2) is from protons with energies below 1 MeV, and that protons with energies greater than 10 MeV make very little contribution. As the thickness of the shielding increases, the curve moves to the right.

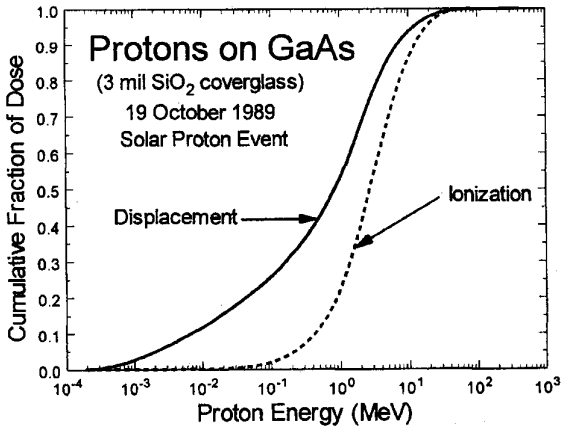

Fig. 8.4. Cumulative fraction of ionizing and NIEL dose as a function of slowed-down proton energy for GaAs covered with a 3 mil thick coverglass made of Si. [MESS97]

8.3 Measurement of Displacement Damage Dose

It is standard practice to measure the DD as a function of proton fluence and energy. At present there is no formally accepted unit of displacement damage dose equivalent to the rad(material) used for TID. There is also no dosimeter for measuring DDD. Instead, the fluence and proton energy are recorded and may be used to calculate displacement damage dose. For the best possible measurements of DDD, it is important to have accurate values of fluence and proton energy.

8.4 Damage Factor

The choice of the proper damage factor to measure is important. For example, in the case of DD in Si CCDs, one may consider reduction in charge transfer efficiency, increase in dark current, or increased noise in the amplifier caused by DD. The choice can lead to differences greater than a factor of two in the predicted degradation level of a CCD.[DALE91]

8.5 Separation of DDD and TID

Certain devices such as optocouplers, are sensitive to both TID and DDD effects. The prospect of qualifying the parts using a combination of ^{60}Co gamma rays for TID and neutrons for DDD instead of protons presents itself. In practice it is not possible. First, accurate NIEL calculations have not been carried done for many materials of interest and there are also problems, referred to in Section 8.1, with NIEL calculations at high proton energies in Si. Second, damage annealing greatly complicates the measurement. For instance, DD in lasers are annealed by charge injection, and TID effects in MOS devices are annealed by neutralization of the traps, particularly at elevated temperatures and positive gate bias. Therefore, using neutrons and gamma rays instead of protons to test for the combination of TID and DD should be avoided.

8.6 Microdosimetry

DD testing of modern devices is complicated by the fact that the devices have thin active regions. Many of the PKAs produced as a result of protons colliding with nuclei at normal incidence will exit the sensitive volume and not contribute to the displacement damage. To avoid the resulting erroneous prediction, the test can be done with protons incident from the back side because those PKAs knocked out of the sensitive volume will be compensated for by PKAs generated outside the sensitive volume and knocked into it. Therefore, modern devices with very thin sensitive volumes should, if possible, be tested with protons incident from the rear and the

front and the relative amounts of damage compared to determine whether this effect does in fact occur.

8.7 Time After Exposure Before The Effects Of DD Measured

In most cases one can do the irradiation and then transport the devices back to the lab for testing. For transport back to the laboratory, all the legs should be shorted together to prevent buildup of electric charge. Most of the vacancy-interstitial pairs recombine within less than a second. The remaining recombination rate is much slower. This is not the case if one is combining DD and TID effects. If significant annealing takes place after irradiation, this is probably an indication that TID has made a major contribution. By including a room temperature anneal, the effects of low dose rate in CMOS parts can be simulated, provided the part has not failed.

8.8 Bias During Exposure

When testing for DD, it is usually not necessary to bias the device during irradiation. Certain devices, however, such LEDs undergo charge-injection annealing so they should be appropriately biased during exposure to the proton beam. The application conditions should be known and the devices tested under the same conditions. However, if the proton testing includes both TID and DD, careful attention must be paid to applying the proper bias because the TID is very dependent on bias.

8.9 Number Of Devices

When testing devices such as Vertical Cavity Surface Emitting Lasers (VCSELs), the variability in the response is so great that one should test on the order of ten devices for good statistics.[MARS99]

8.10 Presence Of Background Neutrons

Neutrons are produced during proton testing at an accelerator. They can, in principle, add to the DD, but in most cases the neutron flux is 10^{-4} times that of protons and so can safely be neglected [BERG97].

8.11 Flux

For most devices, the flux for DD testing is determined in large part by the total fluence required to reach a desired level of damage and by the time (dollars) available for testing. Because most of the recombination of vacancy-interstitials takes place in less than a second, it is not necessary to use low fluxes for which long exposure times would be required.

8.12 Shielding Calculations

There are various programs that calculate the transport of radiation through material including: BRYNTRN, FLUKA, HZETRN, GEANT4, SIREST(NASA Langley uses HZETRN) SHIELDOSE and NOVICE. CRÈME96 calculates a numerical solution to the one-dimensional continuity equation, taking into account both ionization loss and nuclear fragmentation. Limitations to the transport code are 1) does not include neutron production in the shielding, which is important for thick shielding and devices that are sensitive to DD, 2) does not include target fragments, 3) can only use Al shielding material, 4) Si is the only target. NOVICE is the most versatile code because it gives the particle distributions following passage through shielding material.

9.0 Combined Effects Testing

Previous sections have covered the issues associated with testing for proton ionizing dose, displacement damage, and single event effects. Often, a single test article may be sensitive to effects from two or perhaps even all three of these mechanisms. In this section, we consider circumstances in which combined effects must be considered, and explore specific test cases with references and suggestions of how to proceed where it is either known or suspected that combined effects may complicate data collection or interpretation.

9.1 Discrete and Linear Bipolar Technologies

Discrete bipolar transistors may be sensitive to gain degradation from base current leakage increases due to both bulk displacement damage induced introduction of generation centers and also from ionizing dose induced surface states and their associated dark current. As an example of the relative roles of these mechanisms, see the proton damage study reported by Summers, et al. (SUMM87). Their study measured proton energy dependent damage factors, with the goal of using the damage factor as a metric to correlate the Non-ionizing Energy Loss (NIEL) in both n-type and p-type Si. By using 2N2222 NPN devices and 2N2907 PNP devices, both material systems were analyzed using the following relation:

$$1/h_{FE} = 1/h_{FE0} + K(\text{proton energy})\Phi$$

Where $1/h_{FE0}$ is the pre-irradiation reciprocal gain, K is the damage factor, and Φ is the particle fluence. As is discussed in that paper, the above relation only applies to displacement damage, and the response is typically non-linear when proton dose is deposited on virgin devices. To avoid this complication, prior to proton testing, the ionization induced surface leakage effects were examined as a function of collector current by exposing test samples to C0-60 gamma radiation. In doing so, it was demonstrated that the ionization component of the damage could be taken to saturation, and that the surface generated leakage current due to ionization was stable over a period of weeks. Consequently, to guarantee a "pure" response to only the displacement induced bulk leakage effects, the test samples were exposed to from 1.5 to 3.0 Mrad of Co-60 gamma dose before exposing them to protons. Obviously, virgin devices would exhibit a complex nonlinear response not described by the above relation, and the relative sensitivity to bulk damage versus surface leakage will be dependent on the dose, dose rate, and operating collector current. These factors must be taken into account when devising a test plan and in the data analysis phase so that a reliable (or worst case) estimate of performance in a radiation environment can be made.

The susceptibility of linear bipolar ICs varies over a wide range because of significant variations in processing, device design and specific performance requirements [see MARS99 section 3.3.1, and references therein]. In general, it has been found that devices that contain substrate or lateral pnp transistors are most sensitive to displacement damage as a result of degradation of the minority carrier lifetime in the wide base regions (i.e., low f_T, or gain-bandwidth product). Circuit level design also plays a large role. For example, the use of a lateral pnp transistor as a primary input transistor operating at low current levels would be expected to increase the device vulnerability to degradation from displacement damage. A recent study by Rax et al. provides another example of a design practice which results in proton sensitivity [Rax98]. Their test results present data on an operational amplifier that fails its specification limit at an equivalent ionization level that is only 60% of that observed during gamma irradiation [Rax98]. Field oxide effects are thought to be responsible for the ionization related degradation, but the comparison clearly points to the need to consider both ionization and displacement related proton effects. The authors found that the output stage of the circuit is asymmetrical; it sources up to 10 mA, but is only guaranteed to sink 1 mA. It relies on the gain of a single substrate pnp

transistor to sink current from an external load, making it quite susceptible to displacement damage as a direct result of circuit design. In other linear bipolar devices, either ionization or displacement effects may dominate, and both Co-60 and proton testing is recommended if an understanding of their respective roles is needed.

9.2 Optocouplers

Optocouplers are hybrid modules comprised of an LED optical source, a coupling medium, and a detector that is sometimes followed by an amplifier stage. They provide the basic function of DC isolation between circuit blocks, and find widespread application on spacecraft. The primary performance metric is the current transfer ratio (CTR), which is the ratio of the photodetector collector current to the LED forward (i.e., drive) current. There are many different optocoupler designs and applications (digital and linear), and the radiation response is highly dependent on both factors. As a result of on-orbit failures of these devices in military and civilian spacecraft, laboratory investigations have been performed that confirm the important role of displacement damage in device degradation. The failure in the TOPEX/Poseidon mission was due to CTR degradation at equivalent TID levels of 10-20 krad(Si) where about 1/3 of the TID was contributed by protons [Rax96]. Investigations of the radiation response of current optocoupler technology include [Lisc93, John99, DOrd97, Reed98]. To date, optocouplers with amphoterically doped AlGaAs LEDs have displayed the highest sensitivity to proton damage, and modern devices have proved significantly more susceptible than earlier generations [Rose82].

The radiation responses of optocouplers are complicated by several factors that have been considered in the recent work cited, and continue to be investigated. First, the devices are hybrid modules that may exhibit large part to part variability. A given commercial hybrid may have internal components (such as LEDs) that cannot be traced and may from several sources. Second, the observed radiation induced degradation results from a combination of TID and displacement damage mechanisms, and the relative importance depends on the optocoupler design and application. Also, the coupler may be a part of a larger hybrid such as a DC-DC converter, which includes other radiation sensitive components [Reed98]. Third, as described in the previous section, limits in our current understanding of the energy dependence of the NIEL for III-V (and ternary) materials do not permit accurate on-orbit performance predictions, thereby necessitating significant radiation design margins. It is also worthwhile to note that little is known about possible connections between reliability issues such as lifetime and temperature and radiation-induced degradation. Currently, these effects are assumed to be independent. However, we do know that some optocouplers have exhibited a significant CTR temperature dependence, which is an important consideration since operation well above room temperature is not uncommon on spacecraft [Rax96].

The importance of proton testing to evaluate the on-orbit response of an optocoupler is clearly demonstrated in Figure 9.1 which shows greatly decreased CTR for proton as compared to Co-60 irradiation. Rax et al. disassembled two types of optocouplers to investigate the modes of CTR degradation [Rax96]. They found that the CTR performance was primarily determined by the response of the LED to displacement damage, and that the amphoterically doped AlGaAs LED was significantly more susceptible than the GaAlP LED. As is often the case, a higher performance device fabricated with more pristine material is also more radiation sensitive (e.g., CCDs, solar cells, etc.), and an engineering trade of initial performance versus the radiation sensitivity of the device on-orbit must be performed. Displacement damage also affected the phototransistors in each optocoupler studied by Rax et al., with the reduction in photoresponse being a more significant than gain degradation. Optocouplers that use a photodiode (as opposed to a phototransistor) have been observed to have the best performance to date [Reed98]. In

addition, the optical coupling medium can be affected by ionizing dose, and lose coupling efficiency in a manner that is time, temperature, and dose rate dependent.

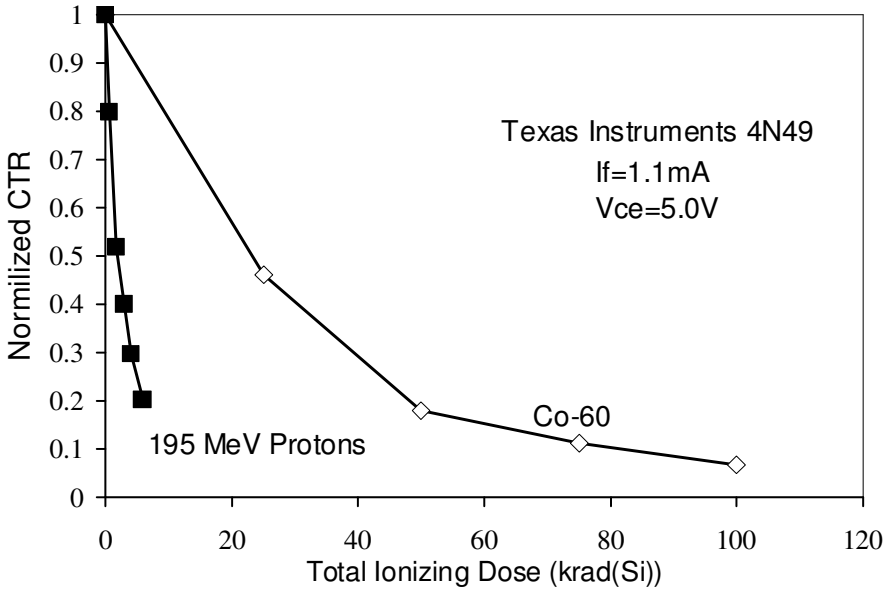

Figure 9.1 Comparison of proton and gamma irradiations clearly demonstrates the importance of both ionizing dose and displacement damage in CTR degradation. Despite the large part to part variability in the pre-irradiation CTR values, similar radiation degradation is observed when the post-irradiation CTRs were normalized to their initial values [Rax96]. After [Reed98].

Application specific laboratory testing is necessary in order to assess on-orbit CTR performance. To begin, we note there is a distinct difference in the performance and electrical characteristics of general-purpose optocouplers, such as those evaluated in [Lisc93, Rax96, Reed98] and those used in linear applications, e.g., DC-DC converters. General-purpose devices exhibit a wide range of CTR values guaranteed to be above a set minimum, whereas those in linear applications have specified CTRs within a narrow range. These differences need to be considered in designing a laboratory evaluation to determine the suitability of such devices for use in space [John99]. In all cases, a proton induced radiation response of an optocoupler will depend on the LED drive current since it impacts the operating point of the phototransistor and therefore, its radiation response. To a lesser extent, the relative contributions of ionizing dose damage versus displacement damage will also depend on the operating conditions.

The importance of application specific testing has been demonstrated by Reed et al. in a study that measured the impact of LED drive current, circuit loading, and the phototransistor collector-emitter voltage (V_{CE}) on the proton induced CTR degradation. The experimental set-up is illustrated in figure 9.2. A radiation induced degradation in the LED light output results in a reduction in the collector current of the phototransistor. If the transistor is in saturation then the change in collector current will be minimal and the CTR will be essentially the same. However, if the same device is operating in the active region, the CTR will be quite sensitive to changes in LED output power. Whether or not the transistor operates in saturation is dependent on the LED drive current and V_{CE}, (which itself depends on the output load). Figure 9.2 illustrates the load dependence of the CTR radiation response for an optocoupler operated with a forward current of 4 mA. It also demonstrates that the common practice of testing at a fixed V_{CE} of 5 V with no

circuit loading significantly over-predicts the CTR degradation, although such data can be used for worst case estimates. Data such as these suggest the mitigation of CTR degradation by operation of the optocoupler at the highest drive current possible while minimizing V_{CE} to obtain the desired I_C for the application [Reed98]. In this case the optocoupler is driven into saturation. However, the trade-off between reliability concerns for LED operation in this mode must be considered. Also, the forward current selected may impact the rate of defect annealing observed in some LEDs.

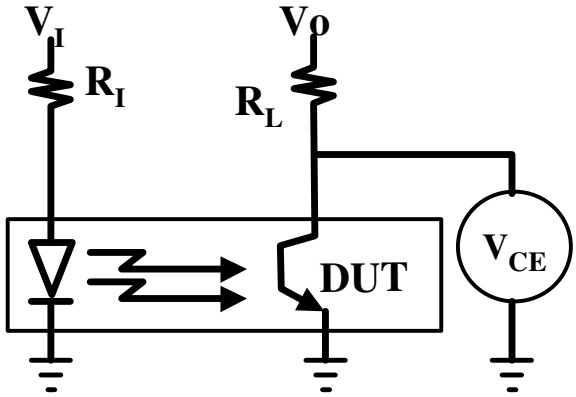

Figure 9.2 CTR measurement setup showing the input voltage and resistance (V_I and R_I), and output voltage (V_O). Two independent power supplies are used to sweep V_I and V_O. Changes in V_I alter the LED drive current. V_{CE} is the difference between V_O and the measured voltage drop across the load resistance (R_L), which can be varied. After [Reed98].

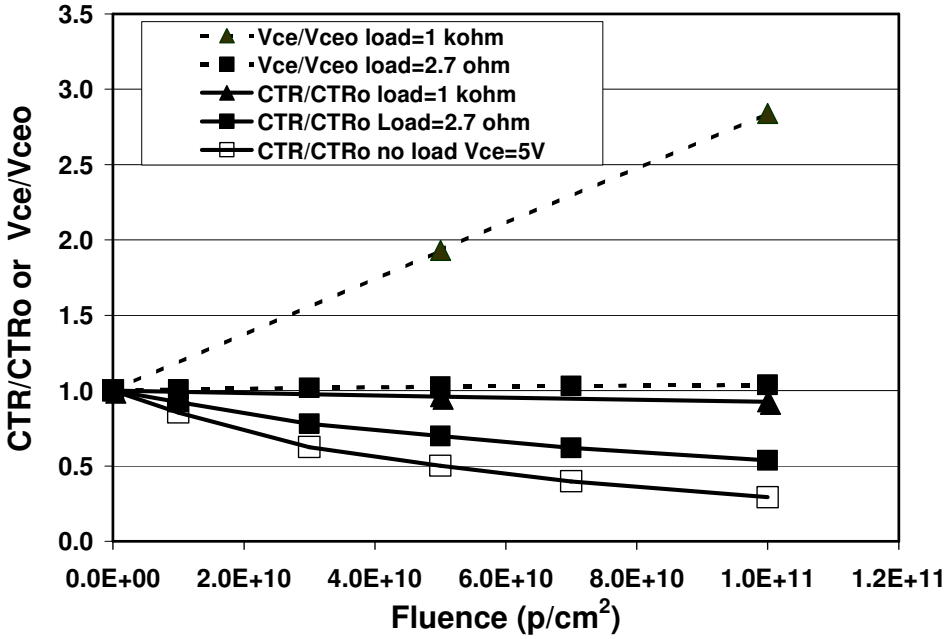

Figure 9.3 Plot of the normalized CTR (solid lines) and normalized V_{CE} (dashed lines) for an optocoupler operated with a forward current of 4 mA and irradiated with 195 MeV protons. In the case of the 2.7 Ω load (with V_{CE} remaining at 0.3 V), the degradation is almost twice that observed for the 1 kΩ load where the degradation is mitigated by an increase in V_{CE}. (V_o was set so that the initial V_{CE} = 0.3 V for both loads.) After [Reed98].

In some cases, laboratory testing has shown the CTR response is dominated by displacement damage to the internal LED. As always, it is important to select the optimal proton test energy (or energies) based on analysis of the shielded proton spectrum relevant to a specific application. The relative importance of displacement damage dose and TID may be assessed by comparing proton and gamma measurements as indicated in figure 9.1. This figure also shows that the CTR response is very nonlinear with proton fluence (or TID or displacement damage dose), so that a damage factor cannot be defined. Nevertheless, the CTR degradation can be plotted versus the equivalent mission fluence or displacement damage dose to assess the end of life performance. (Note that, to first order, the proton testing of CTR degradation can also be considered to incorporate the performance loss from TID effects.) As noted in earlier, the NIEL function for LED materials does not accurately reflect the device response so accurate predictions are not presently possible. In the absence of CTR measurements as a function of proton energy, we have three choices for a function to describe the energy dependence: (1) a calculated NIEL curve, (2) an experimental displacement damage curve from the literature (e.g., the LED data from [Barr95]), and (3) a piecewise "manufactured" worse case damage function. It is hoped that further research to permit a better understanding of the radiation performance of optocouplers and the applicability of the NIEL energy dependence will result in more realistic worst case analyses to facilitate the device selection process. However, there will still remain a wide variation between optocoupler manufacturers concerning issues such as component procurement and coupler design. These issues need to be reflected in the sample size chosen for a radiation test, and significant de-ratings may be necessary to reflect the large part-to-part variations observed for some of these hybrid devices.

9.3 Sensors and Imaging Arrays

Sensor arrays are always subject to single event transients in detector elements and readout circuitry. Also, CMOS devices such as CCDs, CIDs and Active Pixel Sensors can undergo changes in biases due to flatband voltage shifts in gate oxides. Displacement damage to the photodetector can result in increased leakage currents from either bulk of surface defects. In CCDs displacement damage also introduces trapping centers causing loss in the charge transfer efficiency. Furthermore, increases in leakage may influence the measured amount of charge transfer degradation. While CIDs and Active Pixel Sensors may experience flatband voltage shifts and increased leakage currents, they do not suffer from charge transfer degradation. A very detailed discussion of the mechanisms and issues surrounding proton testing and proton effects is provided in [MARS99 and references therein], and portions of this overview are summarized below.

Silicon optoelectronic sensing arrays (visible, UV and x-ray) have been developed for a wide variety of scientific, commercial and military uses in space. They contain a matrix of up to several million photosensitive elements (or pixels) which generally operate by converting the photo-generated charge to a voltage that is multiplexed to a small number of output amplifiers. Present charge coupled devices (CCDs) are available with picoampere dark currents and charge transfer efficiencies (CTE) in excess of 0.999999 per pixel. During the development of these sensors, their susceptibility to ionizing radiation effects has been characterized and hardening solutions have been successfully implemented in many cases. The most commonly used CCD for visible and UV detection is the buried channel device which has a shallow n-type layer implanted below the surface to keep the stored signal charge away from the traps associated with the Si/SiO_2 interface. Such CCDs may be hardened to TID effects either by the use of radiation hardened oxides [Carb93], or by biasing the device so that the silicon surface is inverted so that the interface traps are filled and dark current generation is suppressed. This can be achieved with an extra implantation to form a multiphase pinned device [Jane95], or by shuffling the charge back

and forth between gates within a pixel faster than the surface states can respond (so-called dither clocking) [BURK91, HOPK92]. These techniques typically maintain performance up to ~10-20 krad(Si), and at higher doses flatband voltage shifts can result in increased dark currents when the interface beneath the gate oxide is no longer held in full inversion.

Bulk displacement damage effects often dominate the radiation response in state-of-the-art scientific imagers when operated in natural particle environments up to several krad(Si) [e.g., JANE91, HOLL91b]. The flatband shifts and dark current increases that occur for ionizing dose levels below 10-20 krads(Si) are often not serious, and can be overcome with minor changes in voltages and operating temperature. In contrast, significant CTE losses from displacement damage induced trapping sites are observed for proton exposures of less than 1 krad(Si). Nevertheless, the degree of CTE loss that is tolerable is very application-dependent, and it is still possible for a device to ultimately fail as a result of either TID or displacement damage effects at higher exposure levels. It is important to verify that flatband shifts will not take a device out of inversion prior to the expected mission dose, and also to ensure that the readout amplifier circuitry is robust. A detailed description of proton effects in CCDs may be found in a recent review article [HOPK96] and references therein. Displacement damage degrades CCD performance by decreasing the CTE, increasing the average dark current, by introducing individual pixels with very high dark currents (or "spikes"), and by increasing the noise of the output amplifier. An overview of each of these effects follows.

One of the most important performance parameters for a CCD is the CTE, which is the fraction of signal charge transferred from pixel to pixel during read out. Arrays with 1024 x 1024 pixels (and larger) are routinely used today, and require very low trap densities in order to operate correctly. For example, to reduce signal loss to less than 10% for 1000 pixel-to-pixel transfers, a CTE of at least 0.9999/pixel is necessary. For a typical device with 50 μm^3 pixel volumes, this corresponds to less than one radiation induced defect every ten pixels, which can easily be exceeded during a typical space mission [HOPK96]. If a signal charge is trapped by a proton induced defect, and remains trapped for more than one clock cycle, it will be lost from the signal charge packet. The trapped charge is eventually re-emitted into trailing pixels, and produces a smeared image. It is the interplay between the temperature dependent carrier emission and capture dynamics of the radiation induced traps and the device readout scheme and clocking rates that determine the CTE behavior of an irradiated CCD [MOHS74].

To understand this interplay, we consider the readout procedure for a 2-dimensional CCD array. Signal charge packets are stored in the depletion regions formed underneath a biased gate during the integration period. Since the gate voltage determines the potential well capacity underneath, the signal charge can be moved down the rows in the buried channel by the appropriate sequencing of the gate voltages as indicated in Figure 9.4. The charge is confined laterally to a single row by an implanted channel stop. After each "parallel" transfer of the charge from one pixel to the next, the charge packet is clocked out of the serial register as depicted in Figure 9.4, and the whole process repeated until the imager readout is complete. Unfortunately, the time to read out the serial register is long enough for signal charge to be trapped. The signal charge can subsequently be re-emitted into a trailing pixel thereby degrading the CTE. Since the carrier emission times depend exponentially on temperature, the CTE response of a 2-dimensional CCD array is a strongly temperature dependent. In contrast to the typical area array, the linear CCD with clocking speeds at 1 MHz or more is relatively immune to proton induced CTE degradation. This is because the capture times for key radiation induced defect levels, such as the E-center, are too long relative to the charge transfer rate for the traps to efficiently trap signal charge. Further details of radiation induced CTE degradation are beyond the scope of this

course, but are described in detail in many papers, including [MOHS74, BANG91, DALE93, JANE95, HOPK96].

Unfortunately, efforts to harden CCDs to displacement damage have not been nearly as successful as TID hardening. However, displacement damage effects can be ameliorated using several techniques. CTE loss can be somewhat reduced by substantial cooling (often to about –80 °C), to mitigate the trapping effects of the E-center (and also minimize dark current). As illustrated in Figure 9.5, background charge can dramatically impact the CTE loss by filling the traps so that they do not interact with the signal charge packet. The magnitude of the improvement depends on the signal size, and usually comes at the price of additional noise. Another CTE hardening technique employs an additional phosphorus implant to confine the signal charge to a smaller volume (referred to as a notch or minichannel) so that fewer traps are encountered as the signal charge is read out. Notches may be useful for low signal level applications and some CCD operating conditions, but the efficacy of a notch may vary considerably between manufacturers (or even lots from a single source). Further information concerning mitigation techniques may be found in [HOPK96] and references therein.

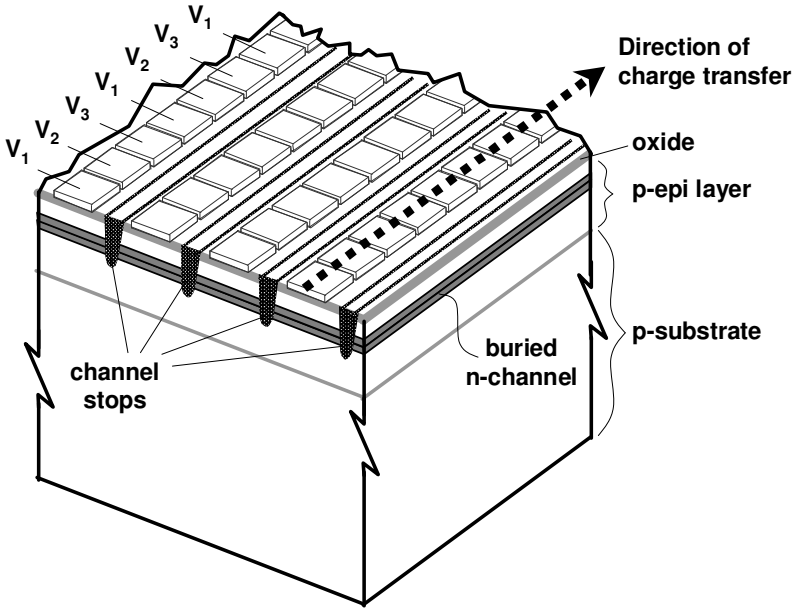

Figure 9.4 Illustration of parallel charge transfer down a row of MOS capacitors. A 3 phase CCD is pictured, in which each pixel is composed of 3 electrodes for charge transfer. The signal charge travels in the buried channel and is restricted to a single row by implanted channel stops.

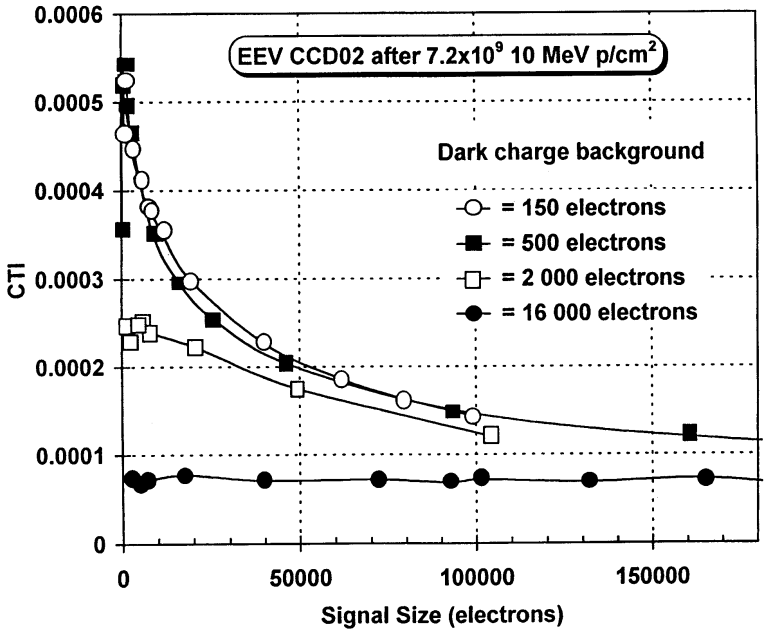

Figure 9.5 The charge transfer inefficiency (CTI = 1-CTE) for a CCD exposed to a proton fluence of 7.2×10^9 cm^{-2}, corresponding to TID of 4 krad(Si). Both the CTI and the efficacy of a dark charge background in CTI reduction are a function of signal size. After [HOPK94b].

For most satellite programs these mitigation techniques are not sufficient, and one must resort to shielding. Unfortunately, high energy protons are not easily shielded against. In fact, quite thick (a cm or more) of high atomic weight shielding (e.g., Ta or W alloys) may be used to minimize displacement damage to the CCD. However, for heavily shielded devices, the displacement damage caused by secondary particles produced in the shielding itself is significant, and in some cases dominant [DALE93]. (Incoming protons may interact with the atoms in the shield material causing nuclear reactions that produce secondary particles such as neutrons and protons.)

The second major effect of proton induced displacement damage on CCDs is the increase in dark current as a result of carrier generation in the bulk depletion region of the pixel. (This assumes that the CCD or CID has a hardened oxide and/or else is run in inversion so that the surface dark current is suppressed.) The average dark current increase is characterized by a damage factor defined as the change in dark current per unit proton fluence.

Although the increase in the mean dark current with proton irradiation is important, the dark current nonuniformity is generally the biggest concern for CCD applications in space. NIEL is an average quantity just as stopping power (or LET) is an average quantity. For ionization effects, the departure from the average dose delivered in a uniform medium is small down to dimensions measured in hundreds of cubic nanometers. This is not the case with NIEL. For Si detector arrays (such as CIDs or CCDs), with pixels measured in the tens or hundreds of cubic microns, the displacement damage sustained by adjacent pixels can vary considerably even though the identical pixels are exposed to the same environment [MARS89]. This nonuniformity is inherent to the statistical nature of the collision kinematics producing the displacement damage and therefore cannot be hardened against.

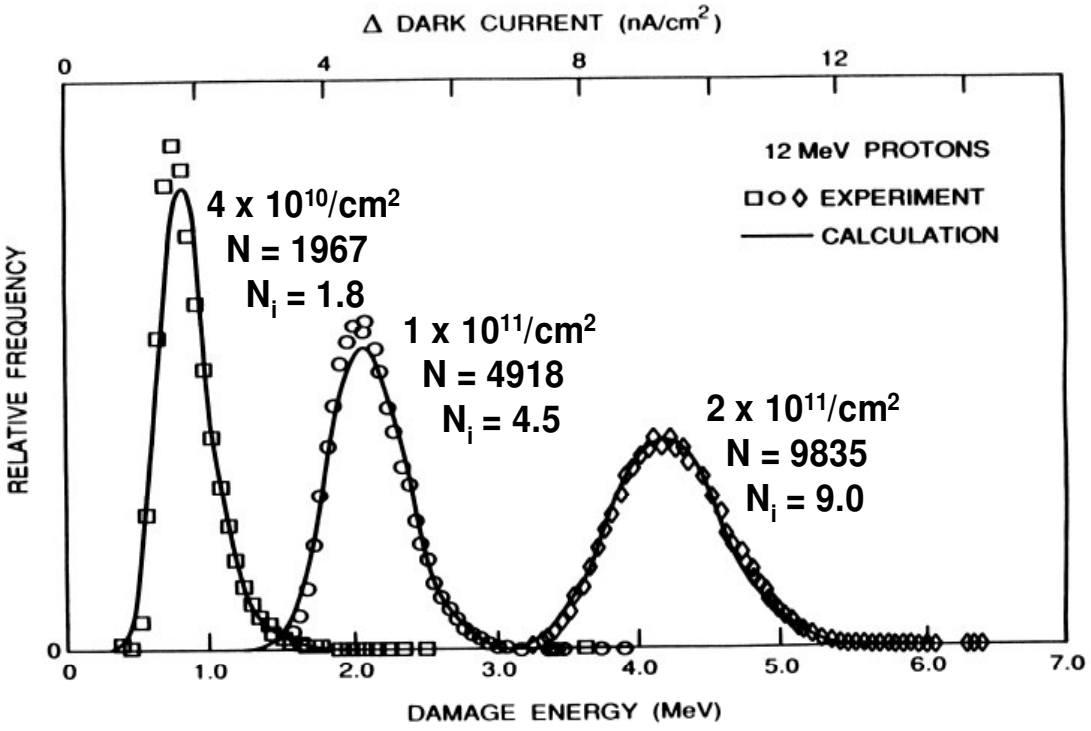

Figure 9.6 CID dark current histograms after exposure to increasing proton fluences. As the number of primary interactions per pixel, N, increases the distribution approaches a gaussian distribution. The high energy tail is produced by very infrequent but large nuclear reaction events. (N_i is the average number of inelastic interactions per pixel.) After [MARS90].

Figure 9.6 illustrates the spread in the dark current increases in individual pixels for a Si CID damaged incrementally by 12 MeV protons. The increase over the pre-irradiation dark current is determined for each pixel and the three histograms are formed from the 61,504 pixel population following each exposure. The high dark current tail is produced from single-particle inelastic nuclear reactions that deposit large amounts of displacement damage energy within the pixel, but are rare enough that relatively few pixels are affected at low fluences. Marshall et al. [MARS89, MARS99 and references therein] have studied the statistics of dark current fluctuations in detail and developed quantitative descriptions of the effect. As seen in Figure 9.6, the analytic predictions (solid lines) of the dark current distributions [MARS90] agree well with the experimental results. At higher proton energies, where the primary recoil ranges approach the pixel dimensions, Monte Carlo techniques are required to model the dark current distributions [DALE94]. In some devices, the presence of even very small high electric field regions can result in dark current distributions that are significantly more skewed than those seen in Figure 9.6 [SROU89, MARS89, MARS90, DALE90, HOPK92]. Improved device design and a reduction of the applied biases can greatly minimize the occurrence of these very high dark current pixels.

The high dark current pixels (so-called spikes) have been observed by several groups in a variety of devices, and also have been noted to have an erratic time dependence [see MARS99 and references therein]. Hopkins and Hopkinson showed that the dark current within a single pixel not only fluctuates in time, but also switches between well-defined levels and has the characteristics of random telegraph noise [Hopk92, Hopk93, Hopk95]. This behavior is illustrated in Figure 9.7 for an EEV CCD irradiated by 10 MeV protons. This type of noise

represents a significant calibration problem for some applications, and this is characteristic of displacement damage, but similar behavior may also be seen in the noise characteristics of CMOS devices from ionization induced interface state traps.

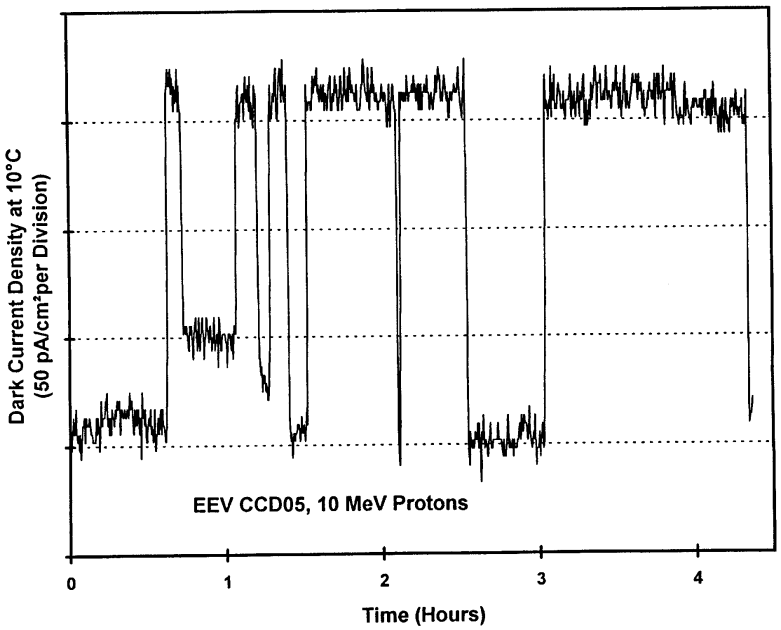

Figure 9.7 After the proton irradiation of a CCD, some pixels show time fluctuations in the dark current with the appearance of random telegraph noise. These measurements were performed on an EEV imager at 10°C. The mean time constants for the high and low states increased at lower temperatures. After [HOPK93].

Despite the extreme sensitivity of CCDs to displacement damage, they are used successfully in space for many applications. Instrument shielding, CCD cooling, careful selection of device architecture and operating conditions, and signal processing all can be used to partially mitigate the proton induced performance degradation. Other types of two-dimensional sensor arrays, such as photodiode arrays, p-channel CCDs [SPRA97] and active pixel sensor arrays show promise for future use in severe space environments.

9.4 CMOS Microcircuits

In general, CMOS devices typically are relatively insensitive to displacement effects, but can suffer from ionizing dose related gate and field oxide leakage paths as well as single event effects. Single event latch-up and several other categories of single event upset may all be possible (e.g. SEU, SEFI, SET, etc,). Characterization of SEE effects must be done carefully since both the functionality of the device and the amount of SEE sensitivity may be affected by the level of oxide related damage. Examples of both increased and decreased SEU sensitivity with increasing ionizing dose have been noted.

Co-60 is most often used for ionizing dose evaluations of CMOS devices as it is relatively inexpensive. To first order, the response of a given device to ionizing dose should not differ significantly if the dose is deposited with protons versus Co-60, but in some cases this is not strictly true [see MARS99 and references therein]. In situations where CMOS devices are monitored in real time during to proton exposure, parametric changes may arise due to gate or field oxide damage from ionization. If device supply currents are used as a metric to determine

device functionality, care must be takes to assure that device operation has not been effected by proton induced single event effects, since latchup or functional interrupt may also result in shifts in device supply currents.

More often, the test objective is to determine the SEU characteristics of a CMOS device to protons, and the unwanted shifts due to ionizing damage to the oxides represent a complication to the measurement of SEU sensitivity. Prior to conducting proton SEU testing, Co-60 based tests or some other indication of the device ionizing dose hardness level should be used as a guide to determine the appropriate number of devices to test. In practice, it is best to carefully monitor the device parametrics during SEU testing and avoid acquisition of data outside the limits of acceptable performance. In addition, a carefully monitored test and appropriate test plan can reveal the dependence of the SEU behavior on the level of oxide damage due to ionization. Often the cross sections for SEU will increase as the dose increases, and this may influence the relative sensitivity of the device for specific categories of errors (e.g. bit flips from 0 to 1 may be favored over 1 to 0 –or vice versa- as the part is damaged.

Petersen has pointed out that the total dose sensitivity of a technology can place practical limitations on the accurate determination of proton SEE cross sections [PETE97]. This can be true for TID hardened parts where assurances of very low cross sections are needed, but it may be much more important for COTS or other unhardened devices for which the TID failure levels may be only a few krad(Si). If the TID failure level of a candidate component is on the order of ~10 krad(Si), then testing on an individual DUT will be limited to that dose. If protons of ~60 MeV are used, this corresponds to a device cross section of ~10^{-11} cm^2. Smaller cross sections cannot be measured with a single device, although they may be important, especially for hard failures and disruptive soft error modes.

The accurate determination of SEE cross sections for important events can require testing of many devices to TID failure levels to get even poor SEE statistics. Such measures may be required when the SEE may lead to catastrophic failure, when many copies of the same device are present on the same satellite, or when many copies of the same device are used in a constellation of identical satellites.

The NASA Hubble Space Telescope offers one such example with its 12 Gbit Solid State Recorder (SSR). The SSR is based on DRAM technology and uses 1440 die with each containing 16 Mbits. Details of the proton SEE response of the individual die are provided in [LABE98], along with a description of in-flight anomalies that indicated proton sensitivity. Prior to flight, testing had been performed with both heavy ions and protons and on flight lot die. In these tests, block errors were identified through heavy ion testing, and the LET threshold was measured at about 5 MeVcm^2/mg. With such a low threshold, protons might be also be expected to cause block errors, but after 3 flight lot die were tested to proton fluences of ~ 3 x 10^{11} (~30 krad(Si)), the devices failed from TID without exhibiting the single event induced block error.

However, after launch, two block errors were noticed and correlated with the proton environment. To understand the source of these errors, further analysis pointed to the need for additional proton testing with a larger sample size. After a second round of testing with a sample size of 100 die, it was determined that protons could lead to the block error condition, and 9 such events were noted on the 100 die sample set. Calculations of the error cross section and expected in-flight error rate showed good agreement with the anomaly rate. Fortunately, for the HST case the block errors were easily corrected with robust Reed-Solomon EDAC protection. The details of this example and others are found in [LABE98].

If the error condition were not easily corrected, or worse, if permanent failure resulted, the condition would not have been predicted with a small test sample set. When large numbers of a given device are flown either on the same spacecraft or across a large number of satellites, correspondingly large samples sizes must be used to assess all possible SEE modes. The exact number will be a function of both the orbit and the TID response of the DUT. If hard failure modes are possible, then large sample sizes may be warranted, even if only one device is to be flown.

9.5 GaAs and other High Speed Devices

High-speed technologies represent a special set of challenges for proton testing. A large body of evidence has shown that GaAs, InP, SiGe, Si bipolar (ECL) and other high bandwidth technologies can exhibit sensitivity to proton induced single event effects, and in addition the level of sensitivity may be a function of the clock or data rate through the device [MARS99 and references therein, REED00]. Since these technologies are not based in CMOS, they are typically not sensitive to parametric failure from total ionizing dose below the 100 krad(Si) range. In fact, GaAs and other III-V devices may show little or no effects to Co-60 ionization levels in excess of 1 Mrad(Si). Even so, care must be taken when measuring the SEU sensitivity to protons, and parametric shifts do not always provide insights into important changes in the response of the device under test.

In [MARS95], measurements of the proton SEU cross section in GaAs HIGFET devices were taken out to levels of greater than 50 Mrad(Si) without noting any parametric shifts or degradation in the part performance. However, significant changes were noted in the SEU cross section, which dropped by over 2 orders of magnitude. The authors explained the result in terms of displacement damage induced changes in the carrier lifetime in the GaAs semi-insulating substrate. By suppressing the carrier lifetime, the charge collection leading to the SEU mechanism was also significantly suppressed, though without affecting device performance. These results suggested that the purposeful introduction of damage with high proton fluences might be used as a means of achieving some degree of SEU tolerance in an otherwise SEU soft device. Here, we note the importance of assuring that the process of measuring the SEU sensitivity does not affect the results, and that many virgin parts may be needed if high fluences are necessary to gain meaningful statistics on the SEU performance, even if the parametric shifts are minimal.

9.6 Hybrids, Board, and Box Level Testing with Mixed Technologies

In hybrid, board level, or box level testing, the variations in technologies may result in a variation in dominate degradation mechanisms from one part to the next. In such cases, test and measurement plans need to be devised carefully so that the most sensitive failure mode can be discovered.

As an example of mixed technology testing, we will consider the case of proton evaluation of a commercial single board computer based on the Power PC-750® processor and manufactured by DY-4, Inc. ®, and this board is shown in front of the UC Davis beamline in Figure 9.8. The SVME-179 board was not irradiated as an entirety during any single exposure, and due to the size of the board this would not have even been possible. Rather, the board area containing active components was divided into smaller regions that were carefully selected and irradiated individually using a collimated proton beam. Three sizes of beam collimators were used for precise irradiation. A list of 25 regions covering all the active components on the board was prioritized according to likelihood of SEL or Total Ionizing Dose (TID) failure and the

importance of gaining information on that/those parts in order to maximize the data in the event of DUT failure before the test ended.

Throughout the course of the series of tests, all regions were irradiated to a cumulative proton fluence of 4 x 10^{10} protons/cm^2 at 63 MeV, which corresponds to an ionizing dose of 5.6 krad(Si). This corresponds to approximately 10x the expected mission fluence based on the intended application. Rather than expose individual parts to this level in the first pass, an initial test round exposed each collimated region to a fluence level of 8.0 x 10^9 protons/cm^2 at 63 MeV, which corresponds to an ionizing dose of 1.08 krad(Si). This corresponded to approximately 2x the expected mission fluence, and the initial test fluence reflected the need to show that the mission needs would be met (for a very benign environment), along with the expectation that this would not exceed the failure levels for the commercial CMOS technologies represented in the ~120 parts on the 2-sided board. Upon successful completion of this first pass, two additional passes were conducted with incremental fluences of 1.2 x 10^{10} protons/cm^2 at 63 MeV and 2.0 x 10^{10} protons/cm^2 at 63 MeV. These later two passes of each exposure region were conducted to gain statistics on SEU events and provide additional confidence in the ability of the board to meet the intended application, but without exposing any single part to a high fluence before some data were collected on all parts.

The overlay of the apertures with the board is shown as Figure 9.9 which also shows how the exposures were grouped into three aperture sizes. Note that the overlay includes both the front-side, backside, and mezzanine board positions, since at 63 MeV negligible attenuation results from penetration of the populated base and daughter boards.

The consideration for a commercial single board computer for satellite applications is not considered without the acknowledgement of some risk of failure. The testing described here does not qualify the board for flight, however is an important step in understanding the risks. Knowledge gained through identification of failure and failure level of a specific part might be used to select an alternate supplier for that part, and improve the chances for mission success. The key point here is that careful selection of exposure levels and the sequence of exposures, including aperture sequence and size, are necessary in planning testing of complex test articles with mixed technologies and unknown failure modes.

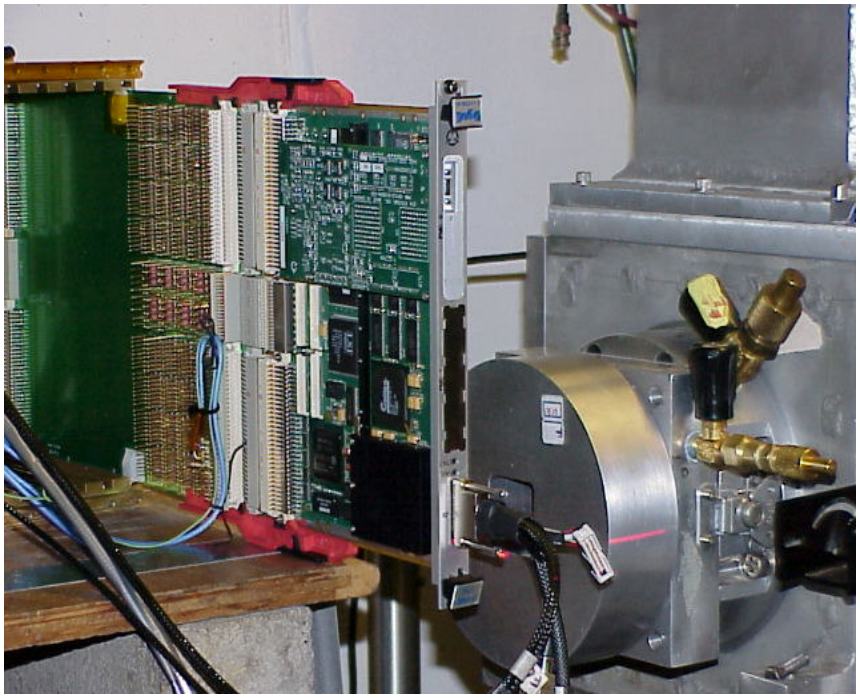

Figure 9.8. Image of the DY-4 179 single board computer operating in a VME chassis and positioned in front of the collimated beam line at the UC Davis proton test facility.

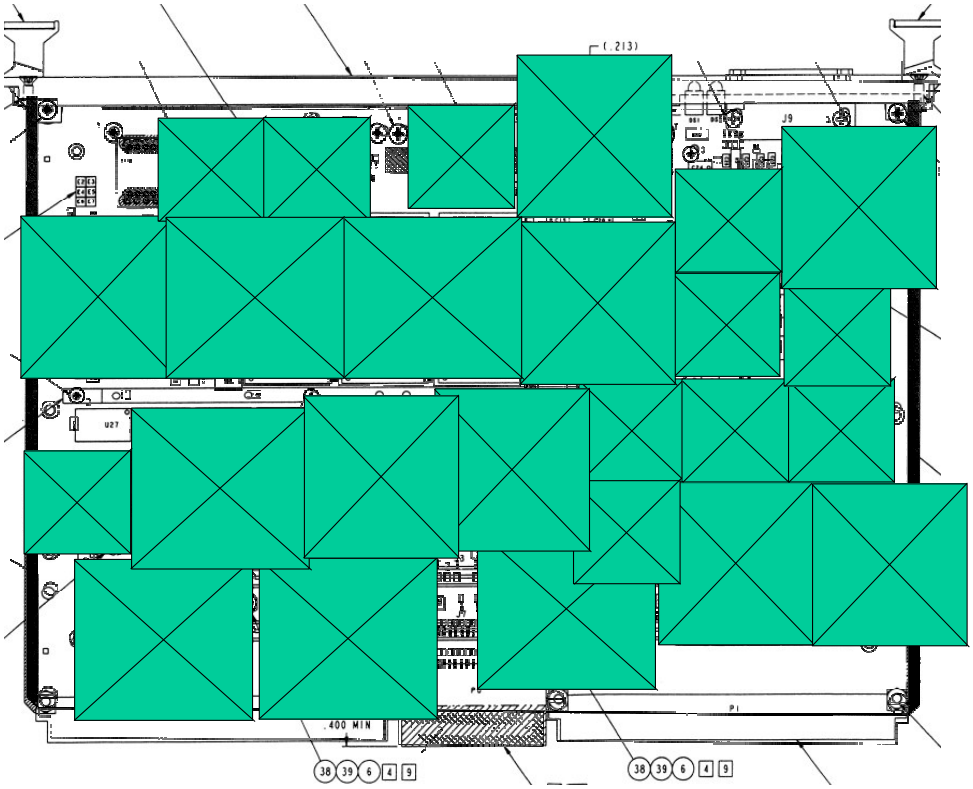

Figure 9.9. Overlay of the DY-4 SVME-179 single board computer with individual apertures used to collimate the proton beam.

10.0 Summary

Our consideration of the practical aspects of proton testing has spanned a range of topics from the availability of various facilities and their contact information, to the basic concerns for dosimetry, the associated radiation safety issues, and the complex response of various technologies to proton damage. Based on lessons we have learned (in many cases the hard way) our summary of the special needs of testing with protons has emphasized the requirement for planning and conducting testing in an environment where one particle leads to three critical device failure mechanisms. Considerations for ionization damage, single event effects, and displacement effects are all important when planning proton tests, and in some cases devices may be subject to two or three of these mechanisms. Further, the microdosimetry of proton damage can be another important consideration when planning tests and the facility and energy at which the testing will be realized.

In presenting the issues associated with proton testing, we have attempted to provide references to the literature and examples where proton testing is necessary to understand the degradation modes and assuring mission success. The technical papers cited here provide essential insights into the basic mechanisms and test approaches needed to conduct testing that allows quantification of the effects in a manner that can be related to the space environment. In our case studies, we have selected topics that are recurring in our endeavors to assure success for NASA missions, and point out the nuisances of the end-to-end experience of planning the test, executing the test, and acquiring the data in a manner that can be analyzed to understand degradation modes and predict the performance on enabling technologies destined to fly with protons. Happy testing!

11.0 Acknowledgements

The authors would like to thank the following individuals who contributed to the preparation of this document:

- Ray Ladbury for insightful and helpful suggestions.
- Scott Messenger (Naval Research Laboratory) for reviewing the section on displacement damage.
- Alan Johnston whose tutorial on displacement damage testing at the Space Parts Working Group Meeting in January 2002 provided some material on combined DD and TID effects.

Need an update on angular measurements

1. References

[AUSM86] G.A. Ausman, "Field Dependence of Geminate Recombination in a Dielectric Medium," Harry Diamond Laboratories Report No. 2097, Adelphi MD (1986).

[BANG91] E.K. Banghart, J.P. Lavine, E.A. Trabka, E.T. Nelson, and B.C. Burkey, "A Model for Charge Transfer in Buried-Channel-Charge-Coupled Devices at Low Temperatures," IEEE Trans. Elect. Dev., Vol. 38, No. 5, pp. 1162-1173, 1991.

[BART97] Janet Barth, "Modeling Space Radiation Environments," Notes from the 1997 IEEE Nuclear and Space Radiation Effects Conference Short Course, Snowmass CO (1997).

[BERG97] G. Berger, G. Ryckewaert, R. Harboe-Sorenson and L. Adams, "CYCLONE – A Multipurpose Heavy Ion, Proton and Neutron SEE Test Site," Abstracts for RADECS 97 W-25, Cannes France (1997).

[BURK91] B. Burke and S.A. Gajar, "Dynamic Suppression of Interface-State Dark Current in Buried Channel CCD Imagers," IEEE Elect. Dev. Lett., Vol. 38, No. 2, pp. 285-290, 1991.

[BURK86] E.A. Burk, "Energy Dependence of Proton-Induced Displacement Damage in Silicon," IEEE Trans. Nucl. Sci. NS-33, 1276 (1986).

[CALV96] Philippe Calvel, Catherine Barillot, Pierre Lamothe and R. Ecoffet, " An Empirical Model for Predicting Proton Induced Upset," IEEE Trans. Nucl. Sci. NS-43, 2827 (1996).

[CARB93] J. Carbone, J. Zamowski, F. Arnold, and J. Hutton, "New Low-Noise Random Access, Radiation Resistant and Large Format Charge Injection Device (CID) Imagers," Proc. SPIE, Vol. 1900, pp. 170-180, 1994.

[CAST01] C.M. Castaneda, "Crocker Nuclear Laboratory (CNL) Radiation Effects Measurement Test Facility," IEEE NSREC Radiation Effects Data Workshop, p. 77-81, 2001.

[DALE90] C.J. Dale, P.W. Marshall, and E.A. Burke, "Particle-Induced Spatial Dark Current Fluctuations in Focal Plane Arrays," IEEE Trans. Nucl. Sci., Vol. 37, No. 6, pp. 1784-1793, 1990.

[DALE93] C.J. Dale, P.W Marshall, B. Cummings, L. Shamey and A. Holland, "Displacement Damage Effects in Mixed Particle Environments for Shielded Spacecraft CCDs", IEEE Trans. Nucl. Sci., Vol. 40, No. 6, pp. 1628-1637, 1993.

[DALE94] C.J. Dale, L. Chen, P.J. McNulty, P.W. Marshall, and E.A Burke, "A Comparison of Monte Carlo and Analytic Treatments of Displacement Damage in Microvolumes," IEEE Trans. Nucl. Sci., Vol. 41, No. 6, pp. 1974-1983, 1994.

[DALY01] Eamonn Daly, "Space Weather and Radiation Effects from Space to Ground," Notes from the RADECS2001 Short Course, Grenoble, France (2001).

[DODD99] Paul E. Dodd, "Basic Mechanisms for Single-Event Effects," Notes from IEEE Nuclear and Space Radiation Effects Conference Short Course, Norfolk VA (1999).

[DORD97] M.D. D'Ordine, et al., "Proton Displacement Damage in Optoelectronic Devices," 1997 IEEE Radiation Effects Workshop Record, IEEE No. 97TH8293, pp. 122-124, 1997.

[DRES98] Paul V. Dressendorfer, "Basic Mechanisms for the New Millenium," Notes from the IEEE Nuclear and Space Radiation Effects Conference Short Course, Newport Beach CA (1998).

[FLEE95] D. Fleetwood " A First-Principles Approach to Total Dose Hardness Assurance," Notes from the IEEE Nuclear and Space Radiation Effects Conference Short Course, Madison WI (1995).

[GARR93] Henry Garrett, "Radiation Environments within Satellites," Notes from the 1993 IEEE Nuclear and Space Radiation Effects Conference Short Course, Snowbird UT, (1993).

[HOLL91b] A. Holland, A. Holmes-Seidle, B. Johlander, and L. Adams, "Techniques for Minimizing Space Proton Damage in Scientific Charge Coupled Devices," Trans. Nucl. Sci., Vol. 38, No. 6, pp. 1663-1670, 1991.

[HOPK92] G.R. Hopkinson, "Cobalt-60 and Proton Radiation Effects on Large Format, 2-D, CCD Arrays for an Earth Imaging Application," IEEE Trans. Nucl. Sci., Vol. 39, No. 6, pp. 2018-2025, 1992.

[HOPK93] I.H. Hopkins and G.R. Hopkinson, "Random Telegraph Signals from Proton-Irradiated CCDs," IEEE Trans. Nucl. Sci., Vol. 40, No. 6, pp. 1567-1574, 1993.

[HOPK95] I.H. Hopkins and G.R. Hopkinson, "Further Measurements of Random Telegraph Signals in Proton-Irradiated CCDs," IEEE Trans. Nucl. Sci., Vol. 42, No. 6, pp. 2074-2081, 1995.

[HOPK96] G.R. Hopkinson, C.J. Dale, and P.W. Marshall, "Proton Effects in Charge-Coupled Devices," IEEE Trans. Nucl. Sci., Vol. 43, No. 2, pp. 614-627, 1996.

[JAFF13] G. Jaffe, "Zur Theorie der Ionisation in Kolonnen," Ann. Phys. (Leipzig) 42, 303 (1913).

[JANE95] J. Janesick, T. Elliott, R. Winzenread, J. Pinter, and R. Dyck, "Sandbox CCDs," Proc. SPIE, Vol. 2415, pp. 2-42, 1995.

[JOHN94] A.H. Johnston, G.M Swift and B.G. Rax, "Total Dose Effects in Conventional Bipolar Transistors and Linear Integrated Circuits," IEEE Trans. Nucl. Sci. NS-41, 2427 (1994).

[JOHN96] A.H. Johnston, "The Influence of VLSI Technology Evolution on Radiation-Induced Latchup in Space Systems," IEEE Trans. Nucl. Sci. NS-43 505 (1996).

[JOHN99] A. H. Johnston and B.G. Rax, "Proton Damage in Linear and Digital Optocouplers," to be presented at RADECS99 and published in the proceedings.

[JONE99] A. Z. Jones, C.D. Bloch, E.R. Hall, R. Hashemain, S. B. Klein, B. von Przewoski, K. M. Murray, and C.C. Foster, "Comparison of Indiana University Cyclotron Facility Faraday Cup Proton Dosimetry with Radiochromic Films, a Calorimeter, and a Calibrated Ion Chamber, IEEE Trans. Nucl. Sci. NS-46, 1762 (1999).

[JORD97] T.M. Jordan, "Report No. EMPC 97.01.02.01," NOVICE: A Radiation Transport/Shielding Code: Users Guide, Jan. 1997.

[JUN01] Insoo Jun "Effects of Secondary Particles on the Total Dose and the Displacement Damage in Space Proton Environments," IEEE Trans. Nucl. Sci. NS-48, 162 (2001).

[JUN01A] Insoo Jun and William McAlpine, "Displacement Damage in Silicon due to Secondary Neutrons, Pions, Deuterons, and Alphas from Proton Interactions with Materials," IEEE Trans. Nucl Sci. NS-48, (2001).

[KOGA89] R. Koga and W.A. Kolasinski, "Heavy ion induced snapback in CMOS devices," IEEE Trans. Nucl. Sci. NS-36, 2367 (1989).

[KOGA93] R. Koga, S.D. Pinkerton, S.C. Moss, S. LaLumondiere, S.J. Hansel, K.B. Crawford and W.R. Crain, "Observation of single event upsets in analog microcircuits," IEEE Trans. Nucl. Sci. NS-40, 1838 (1993).

[KNOL89] G.F. Knoll, Radiation Detection and Measurement, 2nd Ed., p. 216-226, p. 251-260, John Wiley and Sons, (1989).

[LABE98] K.A. LaBel, P.W. Marshall, J.L. Barth, R.B. Katz, R.A. Reed, H.W. Leidecker, H.S. Kim, and C.J. Marshall, "Anatomy of an Anomaly: Investigation of Proton Induced SEE Test Results for Stacked IBM DRAMs," IEEE Trans. Nucl. Sci., Vol. 45, No. 6, pp. 2898-2903, 1998.

[LERA99] Jean-Luc Leray, “Total Dose Effects: Modeling for Present and Future,” Notes from the IEEE Nuclear and Space Radiation Effects Conference Short Course, Norfolk VA (1999).

[LIND63] J. Lindhard, V. Nielsen, M Scharff and P. Thomsen, “Integral Equations Governing Radiation Effects (Notes on Atomic Collisions III),” Mat. Fys. Medd. Dan. Vid. Selsk., Vol. 33, 1 (1963).

[LISC93] H. Lischka, H. Henschel, O. Kohn, W. Lennartz, and H.U. Schmidt, “Radiation Effects in Light Emitting Diodes, Laser Diodes, Photodiodes, and Optocouplers,” RADECS93, IEEE Doc. No. 93TH0616-3, pp. 226-231, 1993.

[MARS89] P. W. Marshall, C. J. Dale, E. A. Burke, G. P. Summers, and G.E. Bender, “Displacement Damage Extremes in Silicon Depletion Regions,” IEEE Trans. Nucl. Sci., Vol. 36, No. 6, pp. 1831-1839, 1989.

[MARS90] P.W. Marshall, C.J. Dale, E.A. Burke, “Proton-Induced Displacement Damage Distributions and Extremes in Silicon Microvolumes,” IEEE Trans. Nucl. Sci., Vol. 37, No. 6, pp. 1776-1783, 1990.

[MARS95] Paul W. Marshall, Cheryl J. Dale, Todd R. Weatherford, Michael La Macchia, and Kenneth A. LaBel, “Particle-Induced Mitigation of SEU Sensitivity in High Data Rate GaAs HIGFET Technologies,” IEEE Trans. Nucl. Sci. NS-42 1844, (1995).

[MARS99] Paul W. Marshall and Cheryl J. Marshall, “Proton Effects and Test Issues for Satellite Designers,” Notes from the IEEE Nuclear and Space Radiation Effects Conference Short Course, Norfolk VA (1999).

[MASS93] L.W. Massengill, “SEU Modeling and Prediction Techniques,” Notes from IEEE Nuclear and Space Radiation Effects Conference Short Course, Snowbird UT, (1993).

[MCLE89] F.B. McLean, H.E. Boesch and T.R. Oldham, “Electron-Hole Generation, Transport, and Trapping,” in Ionizing Radiation Effects in MOS Devices & Circuits,” Ed. By T.P. Ma and P.V. Dressendorfer, John Wiley and Sons, (1989).

[MESS97] S. R. Messenger, M.A. Xapsos, E.A. Burke, R.J. Walters, and G.P Summers, “Proton Displacement and Ionizing Dose for Shielded Devices in Space,” IEEE Trans. Nucl. Sci. NS-44, 2169 (1997).

[MESS01] Scott R. Messenger, Robert J. Walters, Edward A. Burke, Geoffrey P. Summers and Michael A. Xapsos, "NIEL and Damage Correlations for High Energy Protons in Gallium Arsenide Devices,” IEEE Trans. Nucl. Sci. NS-48 (2001).

[MOHS74] A.M. Mohsen and M.F. Tompsett, “The Effects of Bulk Traps on the Performance of Bulk Channel Charge-Coupled Devices,” IEEE Trans. Elect. Dev., Vol. 21, No. 11, pp. 701-711, 1974.

[NOWL92] R.N. Nowlin, E.N. Enlow, R.D. Schrimpf and W.E. Combs, “Trends in the Total Dose Response of Modern Bipolar Transistors,” IEEE Trans. Nucl. Sci. NS-39, 2026 (1992).

[OLDH93] T. Oldham, K.W. Bennett, J. Beaucour, T. Carriere, C. Poivey and P. Garnier, “Total Dose Failures in Advanced Electronics from Single Ions,” IEEE Trans. Nucl. Sci. NS-40, 1820 (1993).

[PEAS01] R.L Pease, M. Simons and P.W. Marshall, “Comparison of pMOSFET Total Dose Response for C0-60 Gammas and High-Energy Protons,” IEEE Trans. Nucl. Sci. NS-48, 908 (2001).

[PETE96] Edward L. Petersen, “Approaches to Proton Single-Event Rate Calculations,” IEEE Trans. Nucl. Sci. NS-43, 496 (1996).

[PETE97] Edward L. Petersen, “Single Event Analysis and Prediction,” Notes from IEEE Nuclear and Space Radiation Effects Conference Short Course, Snowmass CO (1997).

[POIV94] C. Poivey, T. Carriere, J. Beaucour and T. Oldham. "Characterization of Single Hard Errors (SHE) in 1 M-bit SRAMs from Single Ion," IEEE Trans. Nucl. Sci. NS-41, 2235 (1994).

[RAX96] B.G. Rax, C.I. Lee, A.H. Johnston, and C.E. Barnes, "Total Dose and Proton Damage in Optocouplers," IEEE Trans. Nucl. Sci., Vol. 43, No. 6, pp. 3167-3173, 1996.

[RAX98] B.G. Rax, A.H. Johnston, and C.I. Lee, "Proton Damage Effects in Linear Integrated Circuits," IEEE Trans. Nucl. Sci., Vol. 45, No. 6, pp. 2632-2637, 1998.

[ROSE82] B.H. Rose and C.E. Barnes, "Proton Damage Effects on Light Emitting Devices," J. Appl. Phys., Vol. 53, No. 3, pp. 1772-1780, 1982.

[REED95] R.A. Reed and P.J. McNulty, "Effects of Geometry on the Proton SEU Dependence on the Angle of Incidence," IEEE Trans. Nucl. Sci. NS-42, 1803 (1995).

[REED98] R.A. Reed, P.W. Marshall, A.H. Johnston, J.L. Barth, C.J. Marshall, K.A. LaBel, M. D'Ordine, H.S. Kim, and M.A. Carts, "Emerging Optocoupler Issues with Energetic Particle-Induced Transients and Permanent Radiation Degradation," IEEE Trans. Nucl. Sci., Vol. 45, No. 6, pp. 2833-2841, 1998.

[REED00] Robert A. Reed and Ray Ladbury, "Performance Characterization of Digital Optical Data Transfer Systems," Notes from the IEEE Nuclear and Space Radiation Effects Conference Short Course, Reno, NV (2000).

[SAWY76] Donald M. Sawyer and James I. Vette, "AP-8 Trapped Proton Environment for Solar Maximum and Solar Minimum," National Science Center Data Report NSSDC/WDC-A-R&S 76-06, (1976).

[SEXT92] F.W. Sexton, "Measurement of Single Event Phenomena in Devices and ICs," Note from IEEE Nuclear and Space Radiation Effects Conference Short Course, New Orleans, LA (1992).

[SPRA97] J.P. Spratt, B.C. Passenheim, and R.E. Leadon, "The Effects of Nuclear Radiation on P-Channel CCD Imagers," 1997 IEEE Radiation Effects Workshop Record, IEEE No. 97TH8293, pp. 116-121, 1997.

[SROU88] J.R. Srour, "Displacement Damage Effects in Electronic Materials, Devices, and Integrated Circuits," Notes from IEEE Nuclear and Space Radiation Effects Conference Short Course, Portland OR (1988).

[SROU89] J.R. Srour and R.A. Hartman, "Enhanced Displacement Damage Effectiveness in Irradiated Silicon Devices," IEEE Trans. Nucl. Sci., Vol. 36, No. 6, pp. 1825-1830, 1989.

[SUMM87] G.P. Summers, C.J. Dale, E.A. Burke, E.A. Wolicki, P.W. Marshall and M.A. Gehlhausen, "Correlation of Particle-Induced Displacement Damage in Silicon," IEEE Trans. Nucl. Sci. NS-34, 1134 (1987).

[SUMM92] G.P. Summers, "Displacement Damage: Mechanisms and Measurements," Notes from IEEE Nuclear and Radiation Effects Conference Short Course, New Orleans LA (1992).

[TITU96] J.L. Titus and C.F. Wheatley, "Experimental Studies of Single-Event Gate Rupture and Burnout in Vertical Power MOSFET's," IEEE Trans. Nucl. Sci. NS-43, 533 (1996).

[TITU98] J.L. Titus and C.F. Wheatley, "Proton-Induced Dielectric Breakdown on Power MOSFETs," IEEE Trans. Nucl. Sci. NS-45, 2891 (1990).

[WALT01] Robert J. Walters, Scott R. Messenger, Geoffrey P. Summers, Edward A. Burke, Shyam M. Khanna, Diego Estan, S. Erhardt, Hui Chun Liu, Mae Gao, Margeret Buchanan, Anthony J. SpringThorpe, Alain Houdayer and Cosmo Carlone, "Correlation of Proton Radiation Damage in InGaAs/GaAs Quantum Well Light Emitting Diodes," IEEE Trans. Nucl. Sci. NS-48 (2001).

[WINO86] P.S. Winokur, F.W. Sexton, J.R. Schwank, D.M. Fleetwood, P.V. Dressendorfer, T.F. Wrobel and D.C. Turpin, "Total-Dose Radiation and Annealing Studies: Implications for Hardness Assurance Testing," IEEE Trans. Nucl. Sci. NS-33, 1343 (1986).

[WOOD81] S. Wood, N.J. Doyle, J.A. Spitznagel, W.J. Choyke, R.M. More, J.N. McGruer and R.B. Irwin, "Simulation of Radiation Damage in Solids," IEEE Trans. Nucl. Sci. NS-28, 4107 (1981).

[ZIEG96] J.F. Ziegler, J.P Biersack and U Littmark, "The Stopping and Range of Ions in Matter," Pergamon Press, New York (1996).